Physical Association and Periodicity in Quasar Families with SDSS and 2MRS

C. C. Fulton[1], H. C. Arp[2,3], J. G. Hartnett[4]

ABSTRACT

We have used the Sloan Digital Sky Survey (SDSS) data release 7 (DR7) and the 2MASS (Two Micron All Sky Survey) Redshift Survey (2MRS) $K_s \leq 11.75$ mag data release to test for physical association of candidate companion quasars with putative parent galaxies by virtue of Karlsson periodicity in quasar redshifts. We conducted this analysis using the quasar family detection algorithm described in Fulton and Arp, Astophysical J., 754, 134 (2012) and used therein to analyze the 2dF Galaxy Redshift Survey (2dFGRS) and the 2dF Quasar Redshift Survey (2QZ). The SDSS and 2MRS data sets confirm the 2dF results and allow us to examine additional object behaviors also at high significance.

Subject headings: galaxies: active - galaxies: distances and redshifts - quasars: general - redshifts

1. INTRODUCTION

In Fulton & Arp (2012), hereinafter Paper I, we contrasted the ejection-based concept of high quasar redshifts with an intrinsic component against the Standard Model assumption of extragalactic redshifts caused by the expansion of space-time. In Paper I the opposing arguments are introduced in §1 and discussed in §5, and the historical, technical, and usage aspects of Karlsson (1971, 1973, 1977) redshifts are detailed in §4.1 and the Appendix. It is recommended that the reader be familiar with those sections.

[1]Dept of Physics, the University of Western Australia, 35 Stirling Highway, Crawley, WA 6009, Australia; cfulton@socal.rr.com.

[2]Max-Planck-Institut für Astrophysik, Karl Schwarzschild-Str.1, Postfach 1317, D-85741 Garching, Germany; arp@mpa-garching.mpg.de.

[3]Halton Arp passed away in 2013 December. We dedicate this article to him and to his early decade of work on galaxies and subsequent five decades of work on the nature of galaxy and quasar redshifts.

[4]Institute for Photonics & Advanced Sensing (IPAS), and, the School of Physical Sciences, University of Adelaide, Adelaide, SA 5005, Australia; john.hartnett@adelaide.edu.au.

In Paper I we implemented an algorithm that apparently can detect families of quasars that, with very high statistical probability, are each physically associated with a specific parent galaxy at disjoint redshift. We examined the 2dF Galaxy Redshift Survey (2dFGRS) galaxies (Sadler et al. 2002) and the 2dF Quasar Redshift Survey (2QZ) quasars (Croom et al. 2001). We now extend that study to the Sloan Digital Sky Survey (SDSS) galaxies and quasars (York et al. 2000) from the SDSS Seventh Data Release (DR7; Abazajian et al. 2009) and the 2MASS (Two Micron All Sky Survey; Skrutskie et al. 2006) Redshift Survey (2MRS) galaxies from the 2MRS $K_s \leq 11.75$ mag (2MRS11.75) sampling of nearby galaxies (Huchra et al. 2012). There are multiple motivations for the extension:

- we can demonstrate the existence of the Karlsson periodicity signal in the next generation redshift surveys;
- depending on how it is sampled, the SDSS data set is at least an order of magnitude larger than the 2dF $f_s = 0.9$ data set of Paper I;
- the size of the SDSS quasar data set allows us to more definitively measure whether there exists a difference between the respective signals we detect for bright and faint quasars;
- the 2MRS data set allows behavioral examination of uniform human-characterized nearby galaxies, with distinction by morphology in a nearly complete sub-sample.

In §2 we describe the input data sets. In §3 we describe the preparation and usage of redshift distributions. In §4 we describe the test constraints. In §5 we outline the quasar family detection procedure. In §6 we present the primary results. In §7 we discuss the primary results. In §8 we examine the effect of test constraints on the periodicity signal. In §9 we present our conclusions.

2. THE INPUT DATA SETS

We used five input data sets comprised of SDSS galaxies and quasars, 2MRS galaxies, and 2dF galaxies and quasars. The 2dF data sets, used in this paper for comparison, are the 2dF $f_s = 0.9$ galaxy and quasar data sets used in Paper I. The SDSS tests were run with the SDSS galaxies and quasars. We downloaded the SDSS DR7 galaxies from the SDSS Query / CasJobs site[1] with $z_{\rm Conf} \geq 0.95$. To prevent skewing of results due to domination by galaxy clusters, we declustered using a difference in redshift of at least $\delta z = 0.010$ to cull for SDSS galaxies such that only one of any pair of same-redshift galaxies was preserved if they fell within $30'$ of one another. Since there is no unbiased method of determining the relative

association-worthiness of any given galaxy, the algorithm keeps the first encountered galaxy of any given pair.

Avoiding the $z_{\rm Conf}$ flag (Hartnett 2009; Schneider et al. 2010 p. 2369), we constructed a statistical SDSS quasar sample by culling the Schneider et al. (2010) SDSS quasar data set to preserve only uniformly selected quasars using the catalog of quasar properties compiled by Shen et al. (2011) as follows: only quasars with the UNIFORM flag set to 1 (uniformly selected using the target selection algorithm in Richards et al. 2002) were preserved; quasars with the TARGET_QSO_MAG_OUTLIER flag set (stellar outlier) were omitted; and quasars with the TARGET_QSO_REJECT flag set (excluded region) were omitted.

We declustered the 2MRS galaxy[2] data set using $\delta z = 0.010$ and proximity within $30'$. The 2MRS tests were run with the 2MRS galaxies and the SDSS quasars wherever these data sets overlapped, as determined by the existence of at least one instance of a galaxy and a quasar within $30'$ of each other, which yields 8,705 galaxies. We used Table 5 in Huchra et al. (2012) to construct a set of object types, listed in Table 1, for analysis of this area.

Table 1: 2MRS Object Types Used for Analysis

Object Type	Count	2MRS Code	2MRS Type
AGN	6	−9	QSO/AGN
Elliptical	1,085	−7 through −4	All elliptical types & unclassified
Lenticular	1,342	−3 through 0	All lenticular and SO types
Spiral	3,017	1 through 9, 20	All spiral types & unclassified
unbarred	(642)	A	unbarred (A) spiral
mixed type	(249)	X	mixed type (AB) spiral
barred	(657)	B	barred (B) spiral
Irregular	34	10, 11, 16	All irregular types & extragalactic H_{II}
Galaxy	3,221	15, 19, 98	Peculiar, unclassifiable, or unexamined
All galaxies	8,705	...	All of the above

[1]http://casjobs.sdss.org/CasJobs/ ($15.3547 \leq g \leq 27.2335$ after cull, but g not used in tests.)

[2]http://tdc-www.cfa.harvard.edu/2mrs/2mrs_v240.tgz ($3.898 \leq K_s \leq 11.75$ after cull, but K_s not used.)

3. REDSHIFT DISTRIBUTIONS

As in Paper I, to model a real quasar random redshift distribution we binned actual SDSS QSO redshifts with bin size $\delta_z = 0.01$, fitted a curve to the bins, and then binned the curve such that each object in every original bin was represented by its own redshift on the curve, yielding a final smoothed $N(z)$ distribution. Figures 1 and 2 show separate $N(z)$ distributions modeled for each hour of R.A. and 15° of Decl., using all available QSOs drawn from the prepared SDSS quasar data set.

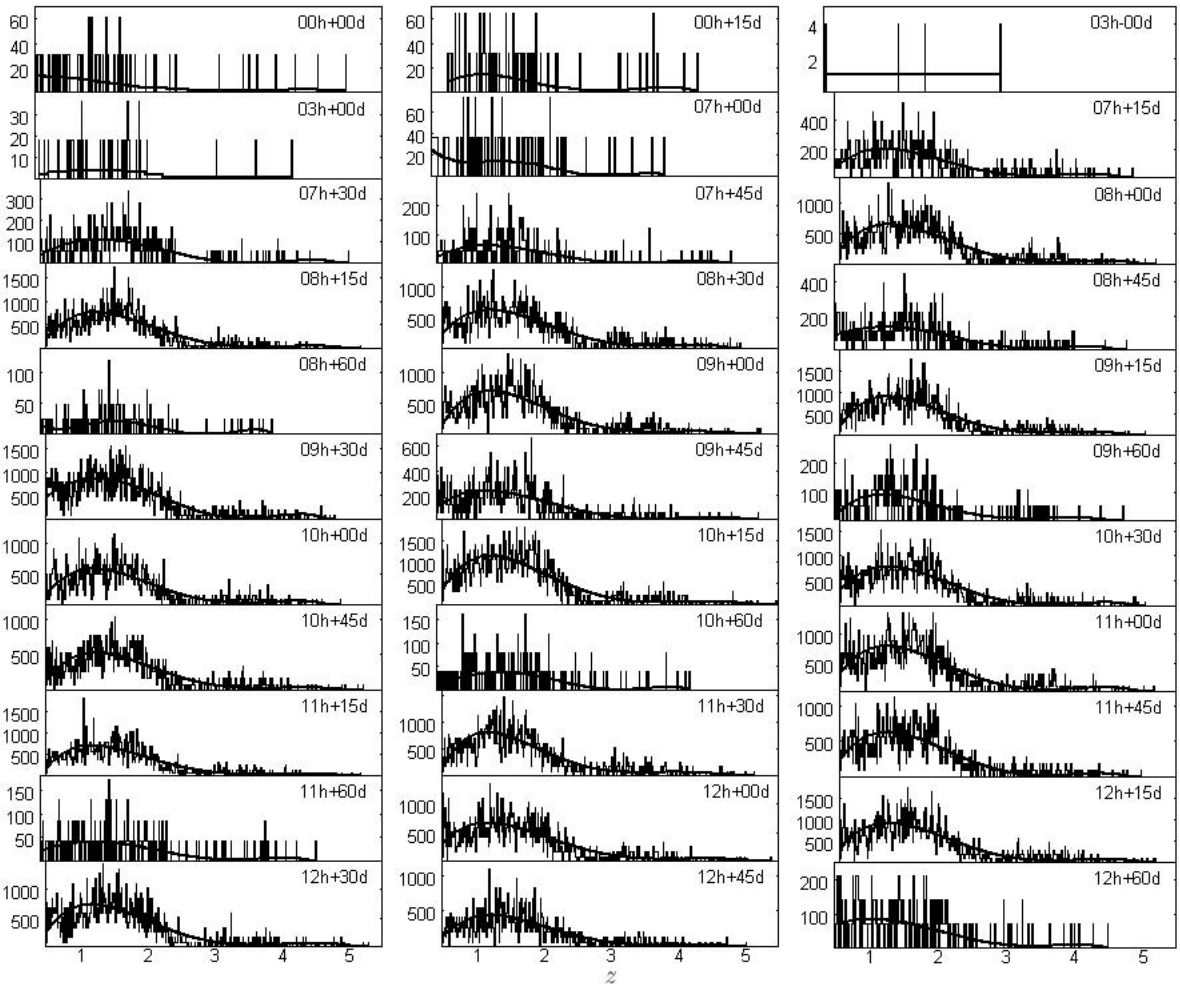

Fig. 1.— SDSS QSO redshifts binned with $\delta_z = 0.01$, curve fitted and smooth-binned for each R.A. hour and 15° of Decl. for hours 0 to 12.

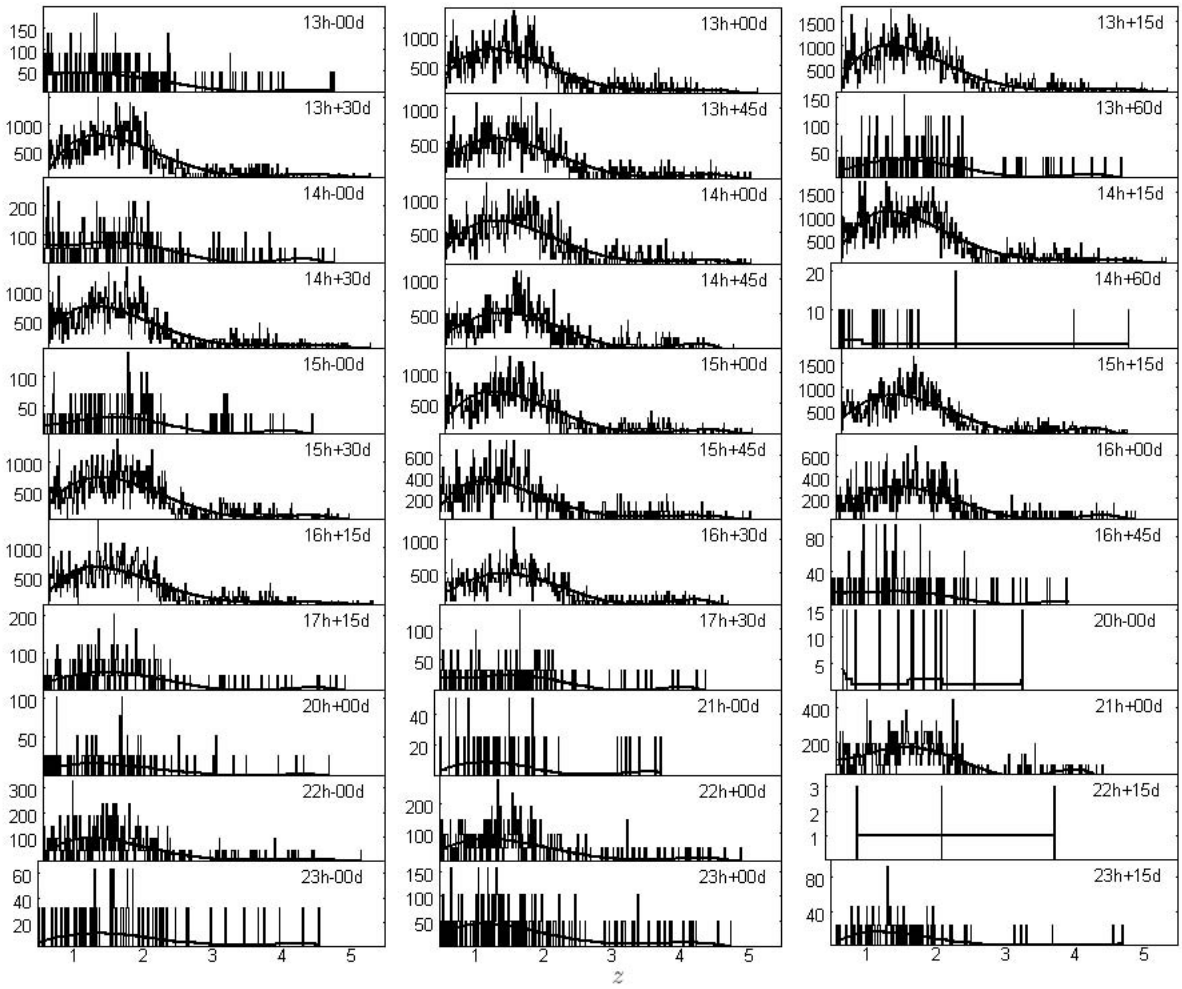

Fig. 2.— SDSS QSO redshifts binned with $\delta_z = 0.01$, curve fitted and smooth-binned for each R.A. hour and 15° of Decl. for hours 13 to 23.

4. TEST CONSTRAINTS

As was the case for Paper I, all of the results presented in this paper were generated using a minimum quasar redshift of $z_{C\,\mathrm{min}} = 0.5$ and a minimum number $N_{\mathrm{min}} = 2$ of quasars that fit the constraints within $30'$ of a galaxy. We accept only quasars that are uniquely associated with a single galaxy, and we ensure effective galaxy declustering. We are also using the same constraints that we developed for Paper I as described therein, except that we have added a third Karlsson corollary constraint, *Karlsson brightness step-up*, that trends a decrease in apparent magnitude of the quasars in a family as their Karlsson number trends lower, the purpose being to increase the number of unique quasar associations and reduce the number of false positive detections. For this constraint, we used the SDSS g or the 2dF b_J apparent magnitude, the comparison always being made between candidate quasar magnitudes from the same survey. The constraint set is summarized in Table 2.

Table 2: Test Constraints

Constraint	Range	Description	Location
Δz_g	0.005− 0.300	z difference outside of which a candidate companion is not considered a member of a group of same-redshift companions — works against actual rather than random redshifts for the control, ensuring that the normal and control will each pass exactly the same quasars through the constraint	Paper I §4.1 p. 5
$\|z_v\|_{\max}$	0.002− 0.120	maximum z velocity of ejection, with z_v computed as the deviation from the closest Karlsson redshift	Paper I Appendix p. 10
Karlsson redshift ordering (corollary #1)		is to accept a quasar if and only if its Karlsson redshift number[a] is less than or equal to that of the preceding accepted quasar, the first otherwise accepted quasar always being accepted by this constraint	Paper I Appendix p. 10
Karlsson redshift velocity stepdown (corollary #2)		is to accept a quasar if and only if its redshift velocity decreases, or steps down, if its Karlsson redshift number[a] is lower than that of the preceding accepted quasar	Paper I Appendix p. 10
Karlsson brightness step-up (corollary #3)		is to accept a quasar if and only if its apparent brightness increases, or steps up, if its Karlsson redshift number[a] is lower than that of the preceding accepted quasar	This Paper §4

[a]The detection algorithm always examines the quasars in order of increasing separation and selects a Karlsson redshift, with the series numbered consecutively from 1 upward starting with the lowest peak at $z_K = 0.06$.

5. QUASAR FAMILY DETECTION PROCEDURE

Here we outline procedural points of the preparation of the input data sets, the equations used in the algorithm from the Appendix of Paper I, the quasar family detection algorithm, the application of test constraints, and the computation of primary results.

- For the 2dF galaxies and quasars the data sets are culled to retain only objects that meet the criteria set out in §2 of Paper I, which includes declustering the galaxies and using the respective 2dF galaxy and quasar redshift completeness masks to achieve a completeness ratio of $f_s = 0.9$ for each data set.

- For the SDSS galaxies and quasars the data sets are culled to retain only objects that meet the criteria set out in §2 of this paper, which includes declustering the galaxies and constructing a statistical sample of quasars.

- For the 2MRS galaxies, the data set is culled to retain only objects that meet the criteria set out in §2 of this paper, which includes declustering the galaxies and the construction of an overlapped sample of 2MRS galaxies with the statistical sample of SDSS quasars.

- For computation of Karlsson redshifts, the one at $z = 1.960$ is used as the anchor and the formula

  $$(1 + z_i)/(1 + z_{i+1}) = 1.228$$

  is used, yielding

  $$z_K = 0.060, 0.302, 0.598, 0.963, 1.410, 1.960, 2.635, 3.464, 4.481, 5.731, ...$$

- The redshift of each quasar is transformed to the reference frame of the putative parent galaxy as per Narlikar & Arp (1993) using

  $$(1 + z_0) = (1 + z_C)/(1 + z_P),$$

  where z_0 is the transformed quasar redshift, z_C is the observed companion quasar redshift, and z_P is the observed redshift of the associated parent object that, by hypothesis, is the ejecting galaxy.

- When processing a candidate companion, the detection algorithm always transforms the redshift of the candidate companion to the rest frame of the putative parent, and this transformed redshift is used in lieu of the redshift of the candidate companion object. This same transformation is applied also to redshifts that have been randomly selected for candidate companions during processing of a control trial.

  The transformed redshift, z_0, of the candidate companion object is then associated with the closest Karlsson redshift, z_K, so that the redshift velocity, z_v—the putative velocity of ejection away from the parent object—can be obtained from the formula (Narlikar & Arp 1993)

  $$(1 + z_v) = (1 + z_0)/(1 + z_K).$$

- For each quasar within $30'$ of each galaxy, and regardless of which constraints are applied for a given test, the algorithm always proceeds with the above computations.

- When a given set of constraints is applied to an entire galaxy/quasar data set, a pair of tests is run, consisting of a single normal test plus an equivalent series of control trials. Just prior to performing each control trial, fresh random redshifts are assigned to each quasar within $30'$ of each galaxy. If a given quasar happens to be within reach of more than one galaxy, a separate random redshift is assigned for each occurrence.

- Constraints are selected from the list described in Table 2. For the Karlsson corollary constraints, it is important to note that the algorithm always examines the quasars in order of increasing separation from a galaxy and selects a Karlsson redshift, with the series numbered consecutively from 1 upward starting with the lowest Karlsson peak at $z_K = 0.06$.

- In addition to applying the chosen constraint set, the algorithm can enforce acceptance of only unique quasar associations, i.e. any quasar that is detected as associated with more than one galaxy is rejected as a companion. The algorithm does a first pass through the data and records single/multiple association information for each quasar. It then does a second pass, using the same logic as the first pass, but this time rejecting any quasar that is not associated with only one galaxy. Except for the additional test described in the second part of §7.1, for all of the tests presented in this paper, this uniqueness option was enabled, guaranteeing that every quasar accepted as a companion is uniquely associated.

- During a test, the control hits are recorded as the floating-point average of all control trials with no round-off. During analysis of the results, the normal hits and unrounded control hits are tallied for the entire data set. The ratio ($\mathsf{hits}_{\mathrm{normal}}/\mathsf{hits}_{\mathrm{control}}$) and sigma ($(\mathsf{hits}_{\mathrm{normal}} - \mathsf{hits}_{\mathrm{control}})/\sqrt{\mathsf{hits}_{\mathrm{control}}}$) are computed from these numbers.

6. RESULTS

For the SDSS galaxies and quasars we ran the same batteries of tests as for Paper I. We applied $\Delta z_g = 0.005$ through 0.025 in increments of 0.005, $|z_v|_{\max} = 0.002$ through 0.060 in increments of 0.002, and the three Karlsson corollary constraints for $N_{\min} = 2$. For comparison, we repeated these tests for the 2dF galaxies and quasars. Table 3 shows the detailed results for the $\Delta z_g = 0.015$ tests using the SDSS and 2dF data sets. In Figure 3, the SDSS galaxy/quasar results are plotted in black, and the 2dF $f_s = 0.9$ galaxy/quasar results are plotted in blue. The 2dF curves are only slightly different from the ones shown in blue in Figure 5 of Paper I, the difference being that the new tests were run with additionally applying the Karlsson brightness step-up corollary constraint described above and in Table 2.

For the 2MRS galaxies and SDSS quasars we ran the same test batteries as for Paper I, but with some additional tests. We applied $\Delta z_g = 0.005$ through 0.030 in increments of 0.005 plus some additional values (0.050, 0.100, 0.200, and 0.300), $|z_v|_{\max} = 0.002$ through 0.120 in increments of 0.002, and the three Karlsson corollary constraints for $N_{\min} = 2$. The 2MRS test batteries were repeated with variations by morphology type in the input galaxy sample. Table 4 shows the detailed results for the $\Delta z_g = 0.015$ tests with all 2MRS galaxies, i.e. whether or not they were typed or classified by Huchra et al. (2012). Table 5 compares the detailed results for the $\Delta z_g = 0.015$ tests with all 2MRS elliptical and lenticular galaxies to the tests with all 2MRS spiral and irregular galaxies. All input galaxy sample variations are plotted in Figures 4a-h. For comparison, the first five curves of Figure 4a are also plotted in Figure 3. The $\Delta z_g = 0.015$ tests are shown in cyan in the respective figures.

The size of the SDSS data set makes possible the detection of groupings of quasar families, some notable examples of which are shown in the sample areas presented in §6.1.

Table 3: Results for Tests Done with $\Delta z_g = 0.015$ and $|z_v|_{\max} = 0.002 \rightarrow 0.060$ Using the SDSS Galaxies and Quasars vs. Using the 2dF Galaxies and Quasars

	SDSS				2dF			
$\|z_v\|_{\max}$	Normal Hits	Control Hits	Ratio	σ	Normal Hits	Control Hits	Ratio	σ
0.002	286	8	35.7500	98.288	139	19	7.3158	27.530
0.004	913	34	26.8529	150.747	340	64	5.3125	34.500
0.006	1,444	69	20.9275	165.531	497	115	4.3217	35.622
0.008	1,848	116	15.9310	160.812	582	167	3.4850	32.114
0.010	2,121	177	11.9831	146.120	631	212	2.9764	28.777
0.012	2,247	240	9.3625	129.551	637	254	2.5079	24.032
0.014	2,351	300	7.8367	118.415	642	288	2.2292	20.860
0.016	2,364	379	6.2375	101.963	628	316	1.9873	17.551
0.018	2,372	455	5.2132	89.870	609	345	1.7652	14.213
0.020	2,379	526	4.5228	80.795	613	371	1.6523	12.564
0.022	2,335	604	3.8659	70.433	625	390	1.6026	11.900
0.024	2,279	684	3.3319	60.986	621	404	1.5371	10.796
0.026	2,259	756	2.9881	54.664	608	417	1.4580	9.353
0.028	2,228	832	2.6779	48.398	592	421	1.4062	8.334
0.030	2,216	903	2.4540	43.694	580	431	1.3457	7.177
0.032	2,213	967	2.2885	40.069	583	441	1.3220	6.762
0.034	2,203	1,027	2.1451	36.696	591	442	1.3371	7.087
0.036	2,178	1,086	2.0055	33.137	561	451	1.2439	5.180
0.038	2,133	1,146	1.8613	29.156	558	453	1.2318	4.933
0.040	2,105	1,191	1.7674	26.484	535	443	1.2077	4.371
0.042	2,089	1,243	1.6806	23.996	524	441	1.1882	3.952
0.044	2,026	1,286	1.5754	20.635	513	435	1.1793	3.740
0.046	2,011	1,317	1.5270	19.123	499	436	1.1445	3.017
0.048	2,001	1,358	1.4735	17.449	495	433	1.1432	2.980
0.050	1,973	1,401	1.4083	15.282	484	432	1.1204	2.502
0.052	1,966	1,445	1.3606	13.706	482	425	1.1341	2.765
0.054	1,933	1,483	1.3034	11.685	470	425	1.1059	2.183
0.056	1,921	1,501	1.2798	10.841	470	423	1.1111	2.285
0.058	1,927	1,533	1.2570	10.063	473	421	1.1235	2.534
0.060	1,933	1,574	1.2281	9.049	464	424	1.0943	1.943

Table 4: Results for Tests Done with $\Delta z_g = 0.015$ and $|z_v|_{\max} = 0.002 \rightarrow 0.120$ Using All 2MRS Galaxies (8,705) and the SDSS Quasars

$\|z_v\|_{\max}$	Norm Hits	Ctrl Hits	Ratio	σ	$\|z_v\|_{\max}$	Norm Hits	Ctrl Hits	Ratio	σ
0.002	6	1	6.0000	5.000	0.062	356	115	3.0957	22.473
0.004	30	2	15.0000	19.799	0.064	360	122	2.9508	21.548
0.006	51	4	12.7500	23.500	0.066	367	127	2.8898	21.297
0.008	83	7	11.8571	28.725	0.068	379	132	2.8712	21.499
0.010	95	9	10.5556	28.667	0.070	381	137	2.7810	20.846
0.012	109	12	9.0833	28.001	0.072	391	144	2.7153	20.583
0.014	127	16	7.9375	27.750	0.074	405	151	2.6821	20.670
0.016	147	18	8.1667	30.406	0.076	414	157	2.6369	20.511
0.018	165	21	7.8571	31.423	0.078	432	164	2.6341	20.927
0.020	180	25	7.2000	31.000	0.080	431	171	2.5205	19.883
0.022	199	28	7.1071	32.316	0.082	449	175	2.5657	20.712
0.024	201	33	6.0909	29.245	0.084	458	183	2.5027	20.329
0.026	213	37	5.7568	28.934	0.086	465	189	2.4603	20.076
0.028	214	40	5.3500	27.512	0.088	474	193	2.4560	20.227
0.030	220	45	4.8889	26.087	0.090	483	199	2.4271	20.132
0.032	222	49	4.5306	24.714	0.092	486	203	2.3941	19.863
0.034	237	53	4.4717	25.274	0.094	493	208	2.3702	19.761
0.036	247	56	4.4107	25.523	0.096	506	215	2.3535	19.846
0.038	259	60	4.3167	25.691	0.098	513	221	2.3213	19.642
0.040	277	66	4.1970	25.972	0.100	515	224	2.2991	19.443
0.042	286	69	4.1449	26.124	0.102	519	225	2.3067	19.600
0.044	294	73	4.0274	25.866	0.104	522	225	2.3200	19.800
0.046	301	78	3.8590	25.250	0.106	526	228	2.3070	19.736
0.048	315	84	3.7500	25.204	0.108	527	231	2.2814	19.475
0.050	323	89	3.6292	24.804	0.110	527	232	2.2716	19.368
0.052	331	94	3.5213	24.445	0.112	527	232	2.2716	19.368
0.054	339	98	3.4592	24.345	0.114	527	232	2.2716	19.368
0.056	339	101	3.3564	23.682	0.116	527	232	2.2716	19.368
0.058	345	104	3.3173	23.632	0.118	527	232	2.2716	19.368
0.060	347	109	3.1835	22.796	0.120	527	232	2.2716	19.368

Table 5: Results for Tests Done with $\Delta z_g = 0.015$ and $|z_v|_{\max} = 0.002 \rightarrow 0.060$ Using the Elliptical and Lenticular (2,427) vs. Using the Spiral and Irregular (3,051) 2MRS Galaxies

	Ellipticals & Lenticulars				Spirals & Irregulars			
$\|z_v\|_{\max}$	Normal Hits	Control Hits	Ratio	σ	Normal Hits	Control Hits	Ratio	σ
0.002	2	1	2.0000	1.000	3	1	3.0000	2.000
0.004	10	1	10.0000	9.000	9	1	9.0000	8.000
0.006	12	1	12.0000	11.000	17	2	8.5000	10.607
0.008	15	2	7.5000	9.192	30	3	10.0000	15.588
0.010	21	3	7.0000	10.392	35	4	8.7500	15.500
0.012	22	3	7.3333	10.970	38	5	7.6000	14.758
0.014	24	4	6.0000	10.000	45	6	7.5000	15.922
0.016	33	5	6.6000	12.522	49	7	7.0000	15.875
0.018	41	6	6.8333	14.289	55	8	6.8750	16.617
0.020	48	7	6.8571	15.497	67	10	6.7000	18.025
0.022	53	8	6.6250	15.910	72	11	6.5455	18.392
0.024	55	10	5.5000	14.230	70	13	5.3846	15.809
0.026	58	11	5.2727	14.171	74	15	4.9333	15.234
0.028	60	12	5.0000	13.856	73	17	4.2941	13.582
0.030	60	13	4.6154	13.035	76	18	4.2222	13.671
0.032	62	15	4.1333	12.135	79	19	4.1579	13.765
0.034	66	15	4.4000	13.168	85	21	4.0476	13.966
0.036	68	17	4.0000	12.369	92	22	4.1818	14.924
0.038	70	18	3.8889	12.257	96	23	4.1739	15.222
0.040	76	19	4.0000	13.077	100	25	4.0000	15.000
0.042	82	20	4.1000	13.864	104	26	4.0000	15.297
0.044	86	22	3.9091	13.645	106	27	3.9259	15.204
0.046	88	24	3.6667	13.064	109	28	3.8929	15.308
0.048	98	26	3.7692	14.120	113	29	3.8966	15.598
0.050	98	27	3.6296	13.664	115	30	3.8333	15.519
0.052	107	29	3.6897	14.484	116	33	3.5152	14.448
0.054	107	29	3.6897	14.484	120	34	3.5294	14.749
0.056	107	30	3.5667	14.058	121	35	3.4571	14.537
0.058	109	31	3.5161	14.009	124	37	3.3514	14.303
0.060	110	32	3.4375	13.789	127	39	3.2564	14.091

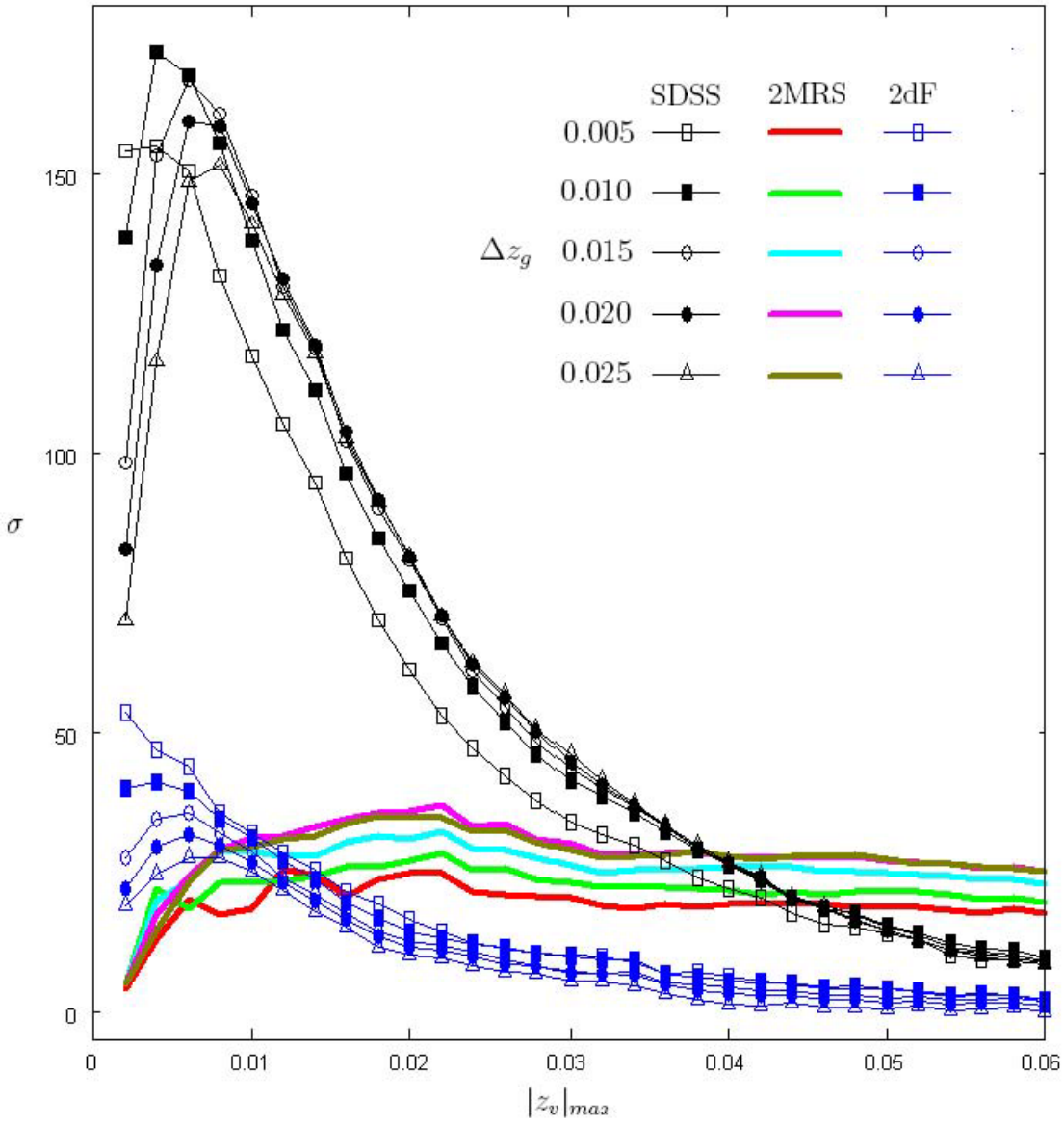

Fig. 3.— Effect on σ of variation of Δz_g and $|z_v|_{\rm max}$ for $N_{\rm min} = 2$ with the SDSS, 2MRS/SDSS, or 2dF data set. Each data point represents the computed sigma for a normal vs. control test pair for the entire SDSS galaxy/quasar (black) data set, the entire 2MRS-galaxy/SDSS-quasar (multi-colored) data set, or the entire 2dF galaxy/quasar (blue) Paper I $f_s = 0.9$ data set. The 2MRS curves are plotted again in Figure 4a, along with some additional curves, out to $|z_v|_{\rm max} = 0.120$. The 2dF curves were generated using the same data sets used to generate the blue curves shown in Figure 5 of Paper I.

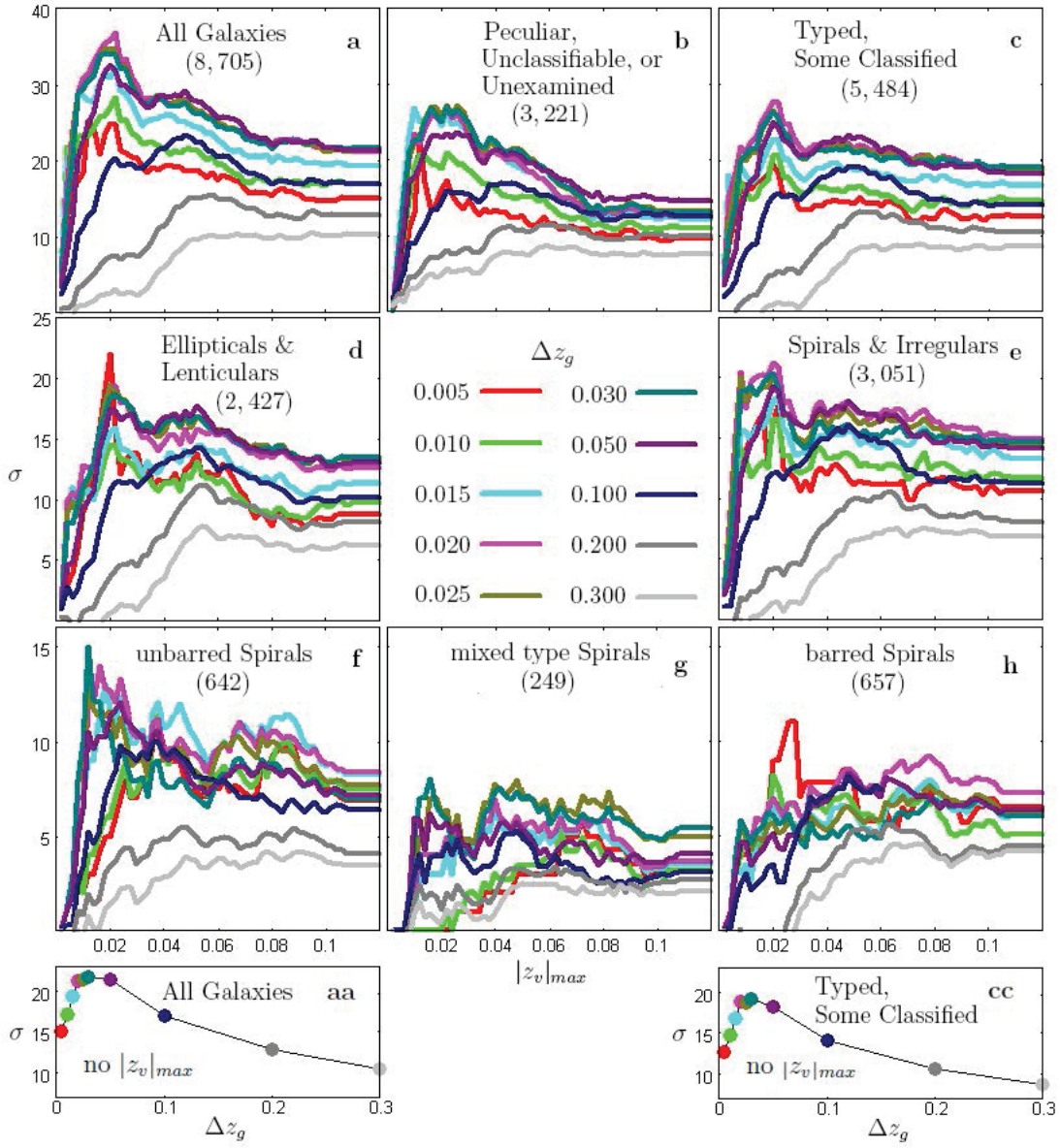

Fig. 4.— Effect on σ of variation of Δz_g and $|z_v|_{\max}$ for $N_{\min} = 2$ with the 2MRS/SDSS data set. Each data point represents the computed sigma for a normal vs. control test pair for the entire 2MRS-galaxy/SDSS-quasar data set. The numbers in parentheses are the counts of galaxies of varied morphology type used as input to the detection algorithm. The range of σ is maintained across each row of plots, and the range is decreased in succeeding rows to compensate for the decreasing input galaxy populations. Panels **aa** and **cc** respectively plot the panel **a** and **c** signals as a function of Δz_g for the case where no $|z_v|_{\max}$ constraint is applied, which is equivalent to $|z_v|_{\max} \geq 0.110$.

6.1. Quasar Families in Sample Areas

In this paper we are for the most part presenting a global view of the data sets and the analyses performed on them. For completeness, in this section we afford the reader the details of actions taken and results obtained by the computer algorithm in sample areas, the impetus being to provide the information and to ameliorate concerns about the correctness of the underlying computations. The sample area results are for the SDSS entry in Table 3 with the highest number of detected quasar families, which was run with $\Delta z_g = 0.015$ and $|z_v|_{\max} = 0.020$, producing 2,379 normal hits and 526 control hits over the whole sky.

When running a test battery, we can optionally generate output files to show the treatment of each putative parent galaxy and its retinue of candidate quasars in an examined individual area. An excerpted screen shot from one of these files is shown in Figure 5 to help describe the content of the files, as presented in the figure caption. The files are verbatim outputs of the inner workings of the family detection algorithm.

Each galaxy is written to the output file in the order processed, and each is followed by a separation ordered list of the candidate quasars and another list of candidate quasar constraint failures. If and only if a family is detected, the galaxy and its detected quasar companions are listed. For example, the output presented in Figure 5 is taken from an output file showing the detection of two families, one for a galaxy with four companion quasars and another for a galaxy with two companions, the former being the one selected for Figure 5. Both families are diagramed in Figure 6.

The algorithm always applies each and every specified constraint to each and every candidate quasar. As noted for the outputs shaded in yellow in Figure 5, each candidate quasar will be listed zero or more times, once for each constraint failure. For the test results presented in this paper, the following possible constraint failures are listed when they occur:

```
Apparent brightness no stepup (Karlsson corollary #3)
Companion not unique          (quasar uniqueness enforcement)
Exceeded |zv| maximum         (redshift absolute velocity maximum)
Redshift not grouped          (redshift grouping)
Redshift velocity no stepdown (Karlsson corollary #2)
Redshift number not ordered   (Karlsson corollary #1)
```

Note that a candidate quasar does not appear in the list of failures if it succeeds every constraint. Note also that the quasar uniqueness enforcement is classified as a constraint for accounting purposes and is therefore listed as a possible constraint failure. It is not a constraint in the usual sense because it is implemented via two passes through the data, as described in §5 in the second to last bullet.

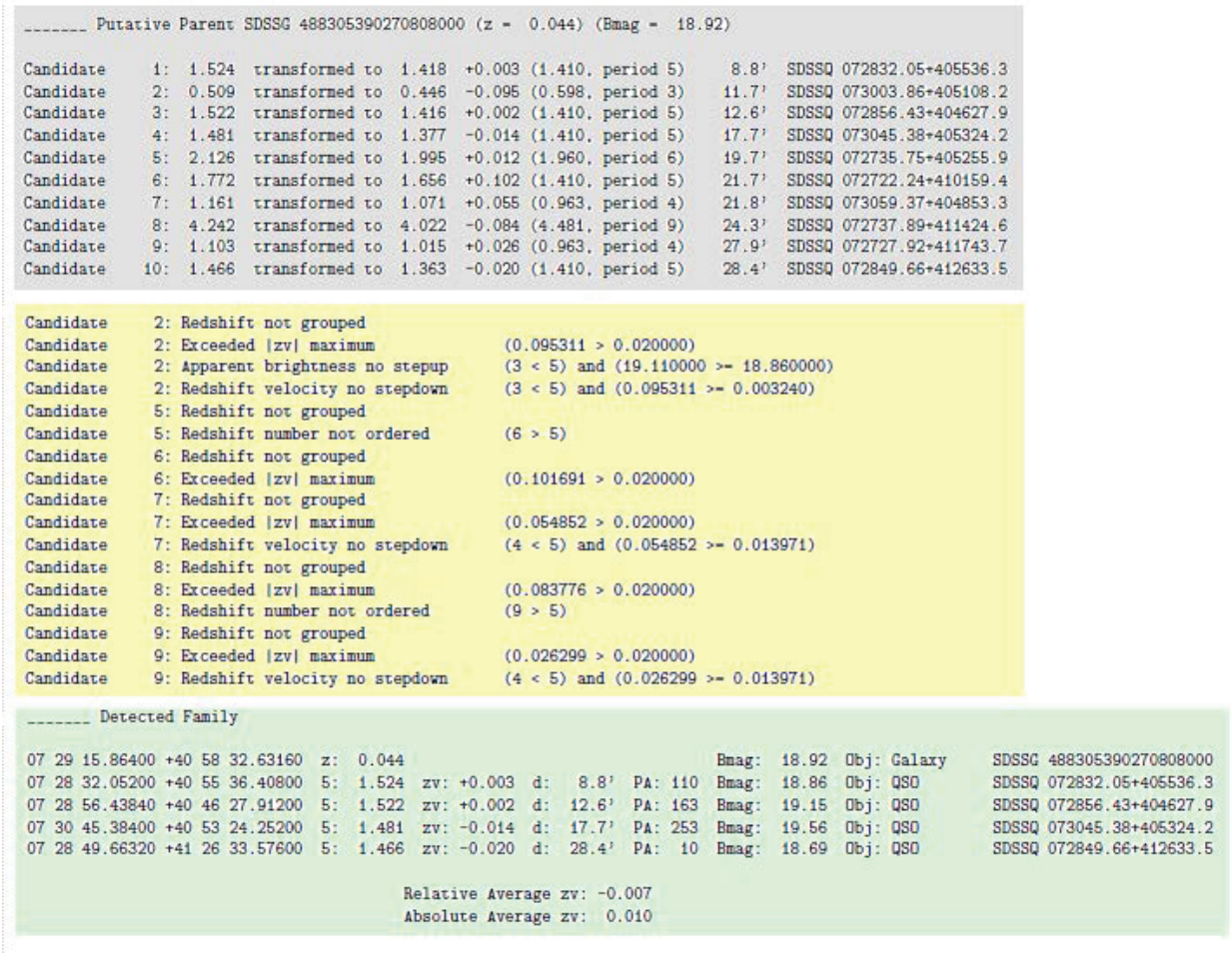

Fig. 5.— Detection output screenshot highlighting key areas of interest in a detection output file. The outputs shaded in gray show the quasar candidates, ordered by increasing separation angle and consecutively numbered, for the galaxy designated in the "Putative Parent" heading. The outputs shaded in yellow show the same numbered quasar candidates zero or more times, once for each rejection by a constraint as described. The outputs shaded in green show the member objects of a detected family under the "Detected Family" heading, which will be present if and only if the putative parent galaxy in question scores a hit.

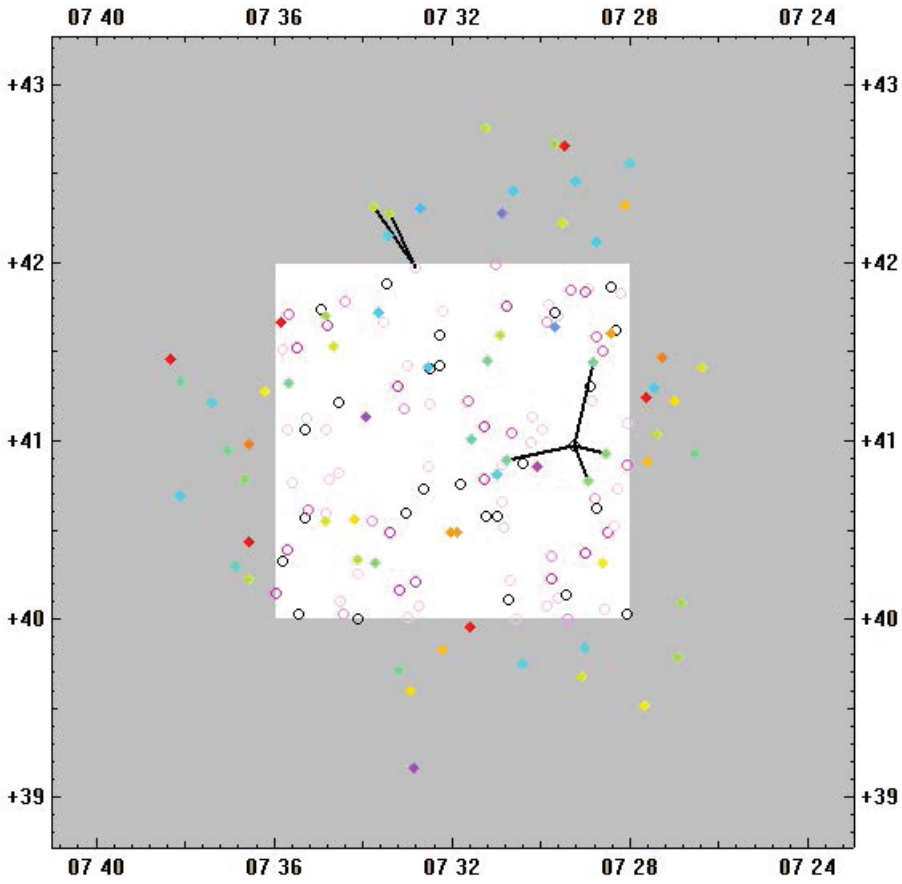

Fig. 6.— Detected families in a 4 square degree area centered at 07h32m00s+41d00m00s. The open circles are galaxies, the filled diamonds are quasars, with lines connecting each galaxy to its detected quasar family members. The object colors indicate stepped redshift increase from black to red over the range $0.0 \leq z \leq 5.5$. The central unshaded area shows the galaxies under examination and the entire area shows the candidate companion quasars.

Figure 7 diagrams and Figure 8 lists the quasar families detected in a 4 square degree sample area that yielded 7 family detections, the highest of all areas examined for the entire SDSS data set. The associated control trials yielded less than one detection, which gives $\sigma = 6$. In this same test, there were 3 areas with $\sigma = 5$, 14 with $\sigma = 4$, and 59 with $\sigma = 3$. *Note that the areas with fewer detections also contribute to the overall signal, and this may or may not include areas in which the control trials outperform the normal test.*

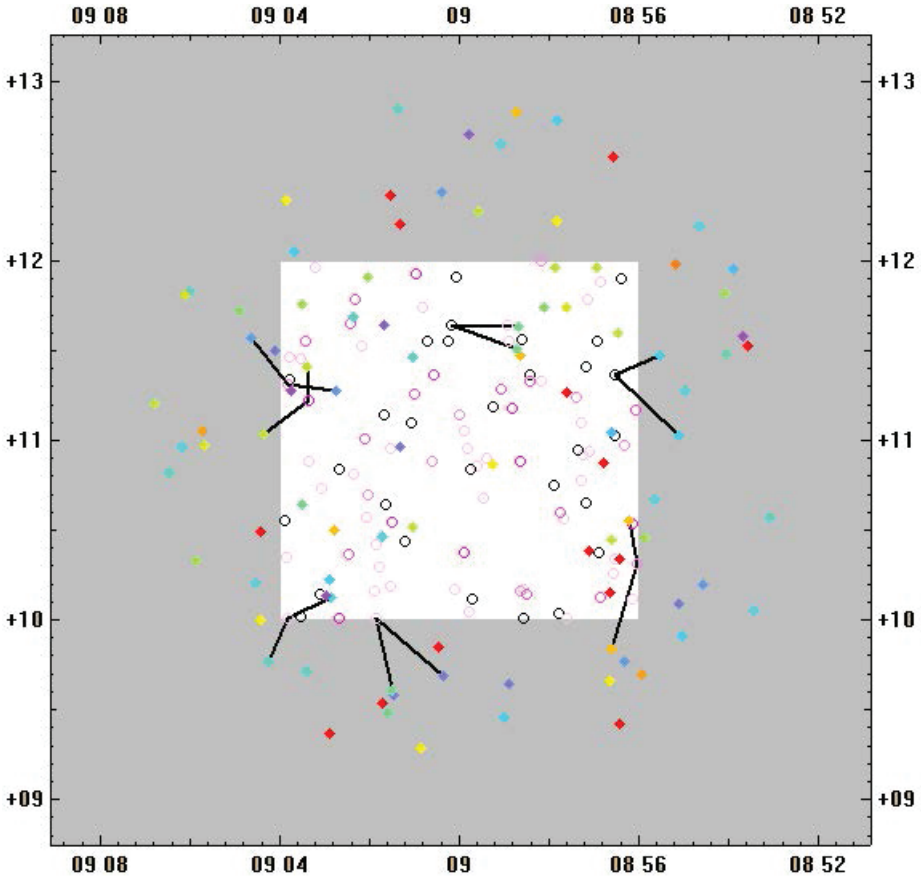

Fig. 7.— Detected families in a 4 square degree area centered at 09h00m00s+11d00m00s. The test results are for the SDSS entry in Table 3 with 2,379 detected families, the highest detection for the entire SDSS data set, run with $\Delta z_g = 0.015$ and $|z_v|_{\max} = 0.020$. The open circles are galaxies, the filled diamonds are quasars, with lines connecting each galaxy to its detected quasar family members. The object colors indicate stepped redshift increase from black to red over the range $0.0 \leq z \leq 5.5$. The central unshaded area shows the galaxies under examination and the entire area shows the candidate companion quasars.

```
08 56 01.64640 +10 18 30.93840  z:  0.277                                  Bmag:  21.09  Obj: Galaxy     SDSSG 489431363238232000
08 56 12.96480 +10 33 01.69200  5:  2.075  zv: -0.001  d:  14.8'  PA: 349  Bmag:  19.33  Obj: QSO        SDSSQ 085612.96+103301.6
08 56 37.12800 +09 50 33.28800  5:  2.088  zv: +0.003  d:  29.3'  PA: 197  Bmag:  18.98  Obj: QSO        SDSSQ 085637.12+095033.2

                                     Relative Average zv: +0.001
                                     Absolute Average zv:  0.002

09 01 52.09680 +10 00 46.17000  z:  0.127                                  Bmag:  19.41  Obj: Galaxy     SDSSG 489431363942875000
09 01 27.06000 +09 34 42.92400  3:  0.825  zv: +0.013  d:  26.8'  PA: 167  Bmag:  18.54  Obj: QSO        SDSSQ 090127.06+093442.9
09 00 21.06720 +09 41 25.51200  3:  0.820  zv: +0.010  d:  29.6'  PA: 131  Bmag:  18.96  Obj: QSO        SDSSQ 090021.06+094125.5

                                     Relative Average zv: +0.012
                                     Absolute Average zv:  0.012

09 03 49.45200 +10 00 21.30120  z:  0.173                                  Bmag:  19.94  Obj: Galaxy     SDSSG 489431364270030000
09 04 15.52080 +09 45 57.70800  4:  1.288  zv: -0.006  d:  15.8'  PA: 204  Bmag:  18.85  Obj: QSO        SDSSQ 090415.52+094557.7
09 02 51.22080 +10 07 29.71200  4:  1.298  zv: -0.002  d:  16.0'  PA:  64  Bmag:  19.20  Obj: QSO        SDSSQ 090251.22+100729.7

                                     Relative Average zv: -0.004
                                     Absolute Average zv:  0.004

09 03 20.61120 +11 13 19.08840  z:  0.408                                  Bmag:  22.08  Obj: Galaxy     SDSSG 725030358801711000
09 03 23.68800 +11 24 40.50000  4:  1.750  zv: -0.005  d:  11.4'  PA: 356  Bmag:  17.91  Obj: QSO        SDSSQ 090323.68+112440.4
09 04 20.85600 +11 02 17.05200  4:  1.739  zv: -0.009  d:  18.4'  PA: 233  Bmag:  19.01  Obj: QSO        SDSSQ 090420.85+110217.0

                                     Relative Average zv: -0.007
                                     Absolute Average zv:  0.007

08 56 32.47200 +11 21 50.01120  z:  0.068                                  Bmag:  18.51  Obj: Galaxy     SDSSG 725030359632183000
08 55 32.70720 +11 28 16.24800  4:  1.062  zv: -0.016  d:  16.0'  PA:  66  Bmag:  19.41  Obj: QSO        SDSSQ 085532.70+112816.2
08 55 07.15200 +11 01 39.68400  4:  1.067  zv: -0.014  d:  29.1'  PA: 134  Bmag:  18.28  Obj: QSO        SDSSQ 085507.15+110139.6

                                     Relative Average zv: -0.015
                                     Absolute Average zv:  0.015

09 00 09.43440 +11 38 38.36760  z:  0.029                                  Bmag:  17.75  Obj: Galaxy     SDSSG 725030360475238000
08 58 40.55280 +11 38 13.12800  5:  1.447  zv: -0.014  d:  21.8'  PA:  91  Bmag:  19.35  Obj: QSO        SDSSQ 085840.55+113813.1
08 58 43.03200 +11 30 19.44000  5:  1.448  zv: -0.013  d:  22.7'  PA: 111  Bmag:  19.23  Obj: QSO        SDSSQ 085843.03+113019.4

                                     Relative Average zv: -0.013
                                     Absolute Average zv:  0.013

09 03 48.30000 +11 18 34.74720  z:  0.223                                  Bmag:  19.65  Obj: Galaxy     SDSSG 725311838799003000
09 02 45.60480 +11 16 19.92000  3:  0.916  zv: -0.020  d:  15.5'  PA:  98  Bmag:  19.21  Obj: QSO        SDSSQ 090245.60+111619.9
09 04 37.50240 +11 34 27.73200  3:  0.918  zv: -0.019  d:  19.9'  PA: 323  Bmag:  19.50  Obj: QSO        SDSSQ 090437.50+113427.7

                                     Relative Average zv: -0.019
                                     Absolute Average zv:  0.019
```

Fig. 8.— Detected families in a 4 square degree area centered at 09h00m00s+11d00m00s as detailed in the Figure 7 caption.

When processed as described in the first paragraph of §2, the SDSS galaxy input data set averages $\sim 226,000/2,744 \simeq 82$ potential families per 4 square degree area. If we use the control case with 526 hits as representative of the null signal, the average expectation over the whole sky is $526/\sim 226,000 \simeq 0.0023$. For a binomial distribution then, the probability of 7 hits for one 4 square degree area is $82!/(7!(82-7)!)\times(0.0023)^7\times(0.9977)^{(82-7)} = 1.089\times10^{-9}$. Under these conditions, the detection of 7 families with this particular constraint set is extraordinary. More generally though, we find it notable that the algorithm does make some detections with a few or more sigma on a local scale for a case that produces at least an order of magnitude larger sigma when the detections are measured over the whole sky.

Figure 9 diagrams and Figure 10 lists the quasar families detected in a 4 square degree sample area that yielded 5 family detections, including one with 3 quasar family members. The associated control trials yielded one detection, which gives $\sigma = 4$.

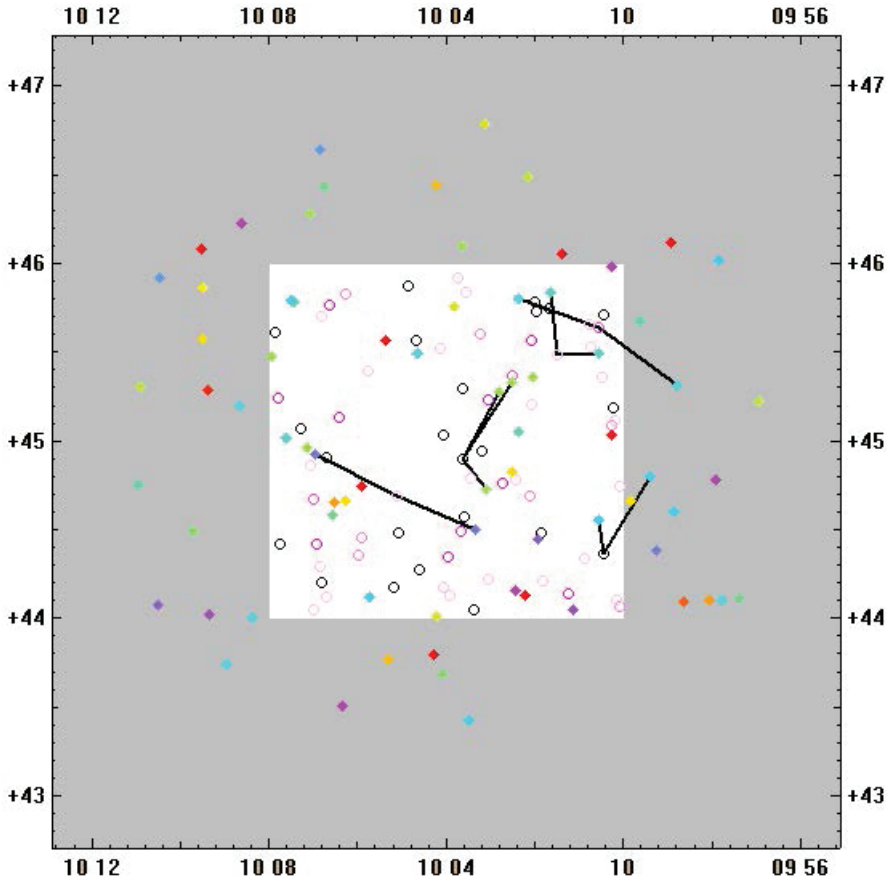

Fig. 9.— Detected families in a 4 square degree area centered at 10h04m00s+45d00m00s. The test results are for the SDSS entry in Table 3 with 2,379 detected families, run with $\Delta z_g = 0.015$ and $|z_v|_{\max} = 0.020$. The open circles are galaxies, the filled diamonds are quasars, with lines connecting each galaxy to its detected quasar family members. The object colors indicate stepped redshift increase from black to red over the range $0.0 \leq z \leq 5.5$. The central unshaded area shows the galaxies under examination and the entire area shows the candidate companion quasars.

```
10 00 27.72720 +44 21 57.02760  z:  0.082                                  Bmag:  19.17  Obj: Galaxy     SDSSG 265375787845156000
10 00 32.75520 +44 33 23.86800  4:  1.118  zv: -0.002  d:  11.5'  PA: 356  Bmag:  19.36  Obj: QSO        SDSSQ 100032.75+443323.8
09 59 23.75280 +44 47 45.49200  4:  1.124  zv: +0.000  d:  28.2'  PA:  24  Bmag:  19.12  Obj: QSO        SDSSQ 095923.75+444745.4

                                     Relative Average zv: -0.001
                                     Absolute Average zv:  0.001

10 00 34.12800 +45 38 06.06120  z:  0.332                                  Bmag:  21.19  Obj: Galaxy     SDSSG 265375787987763000
10 02 21.71520 +45 48 05.97600  3:  1.152  zv: +0.011  d:  21.3'  PA: 298  Bmag:  19.24  Obj: QSO        SDSSQ 100221.71+454805.9
09 58 46.51680 +45 18 51.84000  3:  1.150  zv: +0.010  d:  26.9'  PA: 136  Bmag:  18.63  Obj: QSO        SDSSQ 095846.51+451851.8

                                     Relative Average zv: +0.011
                                     Absolute Average zv:  0.011

10 03 37.30320 +44 53 52.80720  z:  0.084                                  Bmag:  19.50  Obj: Galaxy     SDSSG 265375788306530000
10 03 04.55280 +44 43 35.97600  5:  1.630  zv: +0.007  d:  11.8'  PA: 151  Bmag:  19.04  Obj: QSO        SDSSQ 100304.55+444335.9
10 02 47.29920 +45 16 48.54000  5:  1.629  zv: +0.007  d:  24.6'  PA:  21  Bmag:  19.46  Obj: QSO        SDSSQ 100247.30+451648.5
10 02 29.36640 +45 20 05.92800  5:  1.633  zv: +0.008  d:  28.8'  PA:  25  Bmag:  18.86  Obj: QSO        SDSSQ 100229.36+452005.9

                                     Relative Average zv: +0.007
                                     Absolute Average zv:  0.007

10 05 07.02960 +44 41 33.01800  z:  0.139                                  Bmag:  18.68  Obj: Galaxy     SDSSG 265655857402871000
10 03 20.16480 +44 30 04.21200  3:  0.797  zv: -0.013  d:  22.2'  PA: 121  Bmag:  18.35  Obj: QSO        SDSSQ 100320.16+443004.1
10 06 58.11600 +44 55 31.65600  3:  0.805  zv: -0.008  d:  24.2'  PA: 305  Bmag:  18.06  Obj: QSO        SDSSQ 100658.11+445531.6

                                     Relative Average zv: -0.011
                                     Absolute Average zv:  0.011

10 01 28.77840 +45 28 49.81080  z:  0.150                                  Bmag:  19.09  Obj: Galaxy     SDSSG 265655857746804000
10 00 33.68880 +45 29 42.68400  4:  1.240  zv: -0.008  d:   9.7'  PA:  85  Bmag:  18.66  Obj: QSO        SDSSQ 100033.68+452942.6
10 01 37.48800 +45 50 07.08000  4:  1.245  zv: -0.006  d:  21.3'  PA: 356  Bmag:  19.32  Obj: QSO        SDSSQ 100137.48+455007.0

                                     Relative Average zv: -0.007
                                     Absolute Average zv:  0.007
```

Fig. 10.— Detected families in a 4 square degree area centered at 10h04m00s+45d00m00s as detailed in the Figure 9 caption.

6.2. The Signal as a Function of Quasar Apparent Magnitude

In Paper I we suggested that, under the Standard Model, gravitational lensing is a possible physical explanation for the signal we detect, and that a test of this explanation is to split the quasar sample into bright and faint quasars and look for different signals as a function of apparent magnitude. Ideally, we would like to select arbitrary values for bright and faint cutoffs, but an impartial test requires equivalent bright and faint quasar populations, each roughly equal in magnitude range and in count, and each with a large enough population to obtain a strong signal. On this basis, we selected a bright range of $17.0 \leq g \leq 19.0$, yielding $23,092$ quasars, and a faint range of $19.1 \leq g \leq 21.1$, yielding $22,449$ quasars. In Figure 11 these ranges are indicated respectively with medium and light gray shaded areas on a plot of the entire prepared SDSS quasar $N(g)$ distribution. We then re-ran the tests shown in Figure 3 for the SDSS galaxies and quasars and for all 2MRS galaxies and the SDSS quasars, one test battery each for the bright quasars and one test battery each for the faint quasars. Table 6 compares the detailed bright/faint quasar results for the $\Delta z_g = 0.015$ tests with all SDSS galaxies and Table 7 compares the detailed bright/faint quasar results for the $\Delta z_g = 0.015$ tests with all 2MRS galaxies. The results for all bright/faint quasar tests are shown in Figure 12.

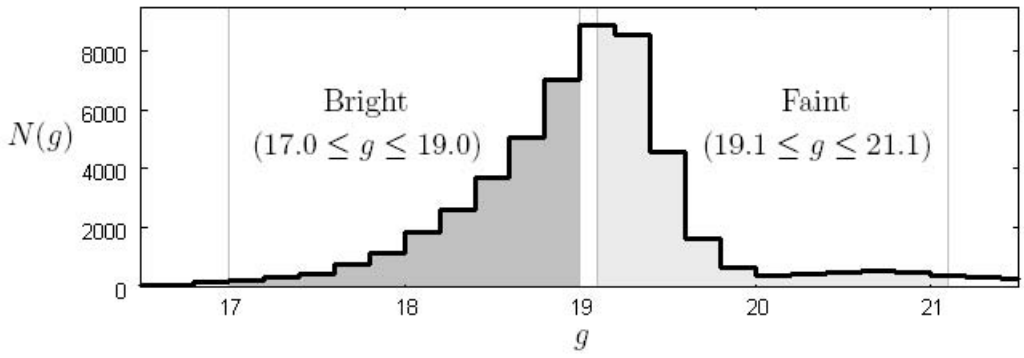

Fig. 11.— Apparent magnitude (g) distribution of the SDSS quasar data set. The shaded areas indicate the equal ranges of magnitude values used to divide the quasars into roughly equal populations of bright (medium gray) and faint (light gray) quasars.

Table 6: Results for Tests Done with $\Delta z_g = 0.015$ and $|z_v|_{\max} = 0.002 \rightarrow 0.060$ Using the SDSS Galaxies and Bright vs. Faint SDSS Quasars

	Bright				Faint			
$\|z_v\|_{\max}$	Normal Hits	Control Hits	Ratio	σ	Normal Hits	Control Hits	Ratio	σ
0.002	54	3	18.0000	29.445	76	1	76.0000	75.000
0.004	209	7	29.8571	76.349	234	8	29.2500	79.903
0.006	363	16	22.6875	86.750	362	18	20.1111	81.082
0.008	461	27	17.0741	83.523	456	29	15.7241	79.292
0.010	545	43	12.6744	76.554	524	45	11.6444	71.405
0.012	606	61	9.9344	69.780	560	59	9.4915	65.225
0.014	660	81	8.1481	64.333	571	73	7.8219	58.286
0.016	672	104	6.4615	55.697	589	90	6.5444	52.599
0.018	676	129	5.2403	48.161	593	112	5.2946	45.450
0.020	670	150	4.4667	42.458	588	136	4.3235	38.759
0.022	670	177	3.7853	37.056	590	158	3.7342	34.368
0.024	651	204	3.1912	31.296	579	182	3.1813	29.428
0.026	641	228	2.8114	27.352	581	205	2.8341	26.261
0.028	633	253	2.5020	23.890	575	228	2.5219	22.981
0.030	629	277	2.2708	21.150	576	252	2.2857	20.410
0.032	636	298	2.1342	19.580	579	278	2.0827	18.053
0.034	640	323	1.9814	17.638	568	306	1.8562	14.978
0.036	640	349	1.8338	15.577	584	327	1.7859	14.212
0.038	632	371	1.7035	13.550	576	348	1.6552	12.222
0.040	624	389	1.6041	11.915	556	366	1.5191	9.931
0.042	617	412	1.4976	10.100	558	383	1.4569	8.942
0.044	604	435	1.3885	8.103	560	401	1.3965	7.940
0.046	594	447	1.3289	6.953	560	418	1.3397	6.945
0.048	579	465	1.2452	5.287	570	434	1.3134	6.528
0.050	574	483	1.1884	4.141	569	451	1.2616	5.556
0.052	570	505	1.1287	2.892	565	465	1.2151	4.637
0.054	577	521	1.1075	2.453	569	478	1.1904	4.162
0.056	563	534	1.0543	1.255	561	490	1.1449	3.207
0.058	573	544	1.0533	1.243	565	498	1.1345	3.002
0.060	583	550	1.0600	1.407	567	509	1.1139	2.571

Table 7: Results for Tests Done with $\Delta z_g = 0.015$ and $|z_v|_{\max} = 0.002 \rightarrow 0.060$ Using the 2MRS Galaxies and Bright vs. Faint SDSS Quasars

	Bright				Faint			
$\|z_v\|_{\max}$	Normal Hits	Control Hits	Ratio	σ	Normal Hits	Control Hits	Ratio	σ
0.002	2	1	2.0000	1.000	2	1	2.0000	1.000
0.004	7	1	7.0000	6.000	4	1	4.0000	3.000
0.006	10	2	5.0000	5.657	8	1	8.0000	7.000
0.008	15	2	7.5000	9.192	18	1	18.0000	17.000
0.010	19	3	6.3333	9.238	22	1	22.0000	21.000
0.012	24	3	8.0000	12.124	25	3	8.3333	12.702
0.014	33	4	8.2500	14.500	28	4	7.0000	12.000
0.016	38	5	7.6000	14.758	32	4	8.0000	14.000
0.018	48	6	8.0000	17.146	39	4	9.7500	17.500
0.020	49	8	6.1250	14.496	41	6	6.8333	14.289
0.022	57	9	6.3333	16.000	45	6	7.5000	15.922
0.024	61	11	5.5455	15.076	44	7	6.2857	13.985
0.026	69	13	5.3077	15.532	49	8	6.1250	14.496
0.028	69	14	4.9286	14.699	49	9	5.4444	13.333
0.030	72	15	4.8000	14.717	51	11	4.6364	12.060
0.032	72	17	4.2353	13.339	50	13	3.8462	10.262
0.034	77	18	4.2778	13.906	55	14	3.9286	10.958
0.036	80	19	4.2105	13.994	62	16	3.8750	11.500
0.038	87	19	4.5789	15.600	68	18	3.7778	11.785
0.040	91	20	4.5500	15.876	71	19	3.7368	11.930
0.042	91	21	4.3333	15.275	73	21	3.4762	11.347
0.044	93	23	4.0435	14.596	76	22	3.4545	11.513
0.046	96	25	3.8400	14.200	85	24	3.5417	12.452
0.048	104	28	3.7143	14.363	86	25	3.4400	12.200
0.050	109	31	3.5161	14.009	91	26	3.5000	12.748
0.052	115	32	3.5938	14.672	95	28	3.3929	12.662
0.054	117	32	3.6563	15.026	98	28	3.5000	13.229
0.056	119	35	3.4000	14.199	100	29	3.4483	13.184
0.058	123	37	3.3243	14.138	105	31	3.3871	13.291
0.060	126	38	3.3158	14.275	109	33	3.3030	13.230

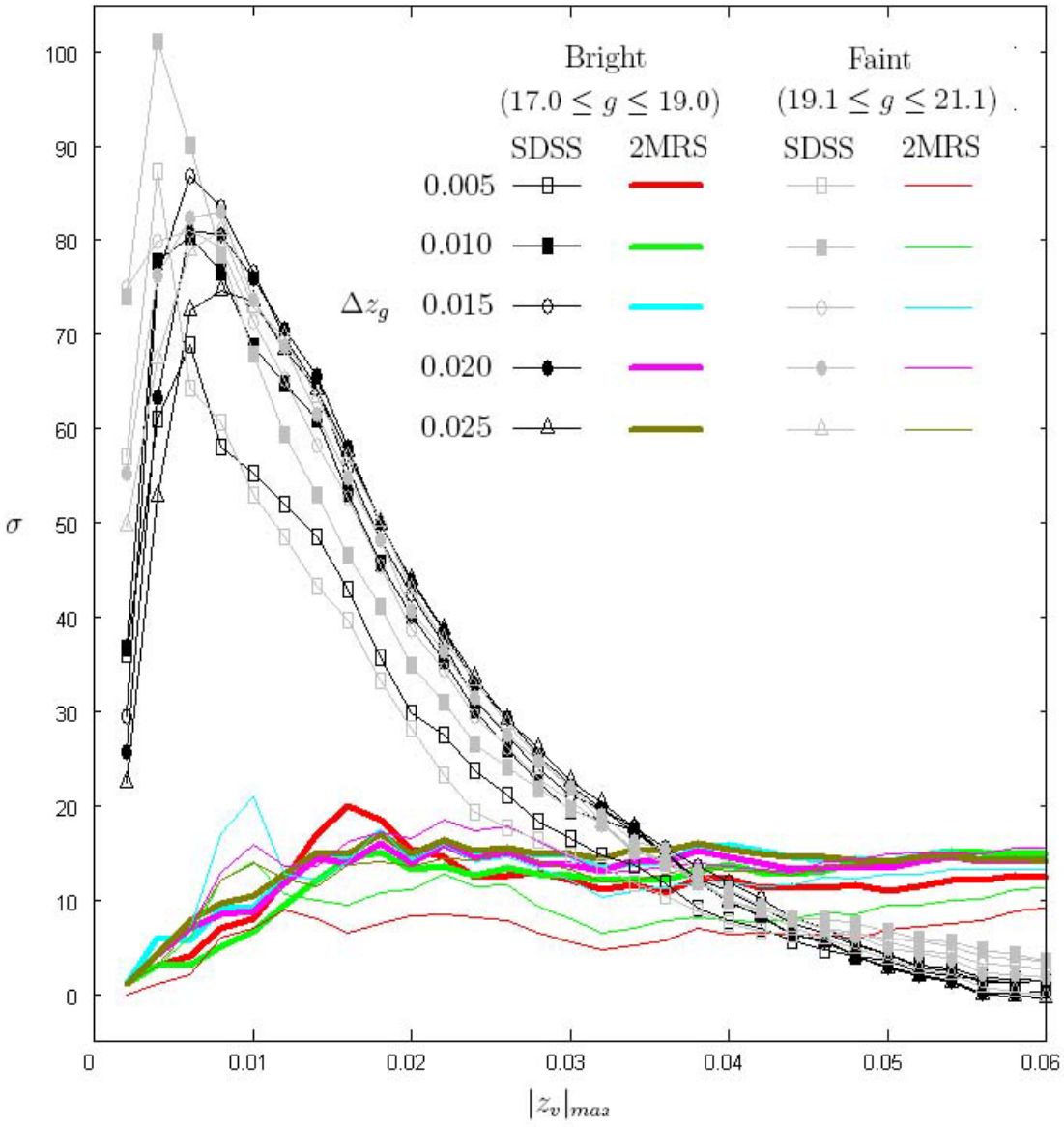

Fig. 12.— Effect on σ of variation of Δz_g and $|z_v|_{\max}$ for $N_{\min} = 2$ for bright and faint SDSS quasars. The tests for the curves shown in Figure 3 were repeated for SDSS galaxies and bright (black) and faint (gray) SDSS quasars and for 2MRS galaxies and bright (heavy multi-colored) and faint (light multi-colored) SDSS quasars.

7. DISCUSSION

From the batteries of curves shown in Figure 3 we make the following observations about the comparison of the quasar family detection results for SDSS (SDSS quasars and galaxies), 2MRS (SDSS quasars and 2MRS galaxies), and 2dF (2dF quasars and galaxies).

1. The curve envelopes for the SDSS and 2dF data sets are very similar, both reaching σ maxima at $|z_v|_{\max} \simeq 0.006$. The SDSS produces a stronger signal throughout the $|z_v|_{\max}$ range in direct proportion to its larger populations of both quasars and galaxies.

2. The 2MRS curve envelope is also narrow throughout the $|z_v|_{\max}$ range, though it is not as tight as the SDSS and 2dF envelopes, reaching σ maxima at $|z_v|_{\max} \simeq 0.022$.

3. For all three data sets, the curve envelope exhibits a steep drop-off from σ maximum that finishes at $|z_v|_{\max} \simeq 0.030$. For the SDSS and 2dF data sets, the drop-off continues to an eventual disappearance of the signal, whereas for the 2MRS data set, the continuation of the drop-off is mild and rides to an eventual constant signal as discussed further in Item 5 below.

From the batteries of curves shown in Figures 4a-h, aa, and cc, we make the following observations about the analyses of SDSS quasars around 2MRS galaxies.

4. The periodicity signal is robust ($\sigma \geq 10$) over most of the $|z_v|_{\max}$ range for $\Delta z_g \leq 0.200$ in Figures 4a-c and for $\Delta z_g \leq 0.100$ in Figures 4d and e. The signal is weaker but still strong for $\Delta z_g \leq 0.100$ in Figure 4f.

5. A value of $|z_v|_{\max} \sim 0.110$ is effectively a maximum useful value because in z_v-space, there is always an available Karlsson redshift within $z_v \sim \pm 0.1$, regardless of the value of the transformed redshift. Therefore, when the $|z_v|_{\max}$ constraint exceeds ~ 0.110, the periodicity signal is asymptotic to a constant value that is determined by the value of the Δz_g constraint. This is true for all cases shown in Figures 4a-h and is *the direct result of the Karlsson corollary constraints*, such that the Karlsson periodicity signal is manifest irrespective of the determined ejection velocity. To illustrate this, panels **aa** and **cc** of Figure 4 show the signal as a function of Δz_g with no $|z_v|_{\max}$ constraint applied. The asymptotic portion of the signal is robust ($\sigma \geq 10$) for $\Delta z_g \leq 0.200$ in Figures 4a-c and for $0.010 \leq \Delta z_g \leq 0.100$ in Figures 4d and e. The asymptotic portion of the signal is weaker but still strong for $\Delta z_g \leq 0.100$ in Figures 4f and h. In short, the signal is robust for a very wide range of Δz_g values, indicating the detection of at least some quasar family members of very different redshift within a given family.

6. From visual inspection of Figures 4d and e, the overall signal of the spiral/irregular galaxy sub-sample appears to be somewhat stronger than that of the elliptical/lenticular galaxy sub-sample, but the input population of the former is a quarter larger. The actual difference can

be quantified using the formula for σ given in §1 and normalizing the normal and control hits by the ratio of the input galaxy populations. With the adjustment factor of $\sqrt{3,051/2,427}$ applied to the elliptical and lenticular galaxy sigmas in Table 5, the elliptical/lenticular sub-sample on average yields the same signal as the spiral/irregular sub-sample.

7. In spite of their smaller input populations, the unbarred (642), mixed type (249), and barred (657) spiral galaxy sub-samples yield healthy signals. The unbarred and barred spirals, with comparable input populations, form fairly well defined σ envelopes, but the unbarred spirals exhibit a clearly stronger signal across the entire $|z_v|_{\rm max}$ range for $0.015 \leq \Delta z_g \leq 0.050$. Probably due to the mixed type spirals having the smallest input population, their curves are more ragged, and although there is an envelope, the signal is considerably damped across the entire $|z_v|_{\rm max}$ range. All of these results could be clarified if and when the unexamined half of the Huchra et al. (2012) galaxy data set is visually examined.

8. The tests for all 2MRS galaxies (Figure 4a) produce the highest significance and also the largest numbers of detected quasar families, but numbering only a few hundred (220 for the test with $\Delta z_g = 0.015$ and $|z_v|_{\rm max} = 0.030$) out of thousands of input galaxies (8,705). There are two factors contributing to this outcome: since the constraint set is intentionally designed to increase unique quasar associations and reduce false positives, some real associations will be rejected by the algorithm; the episodic evolution of quasar families around galaxies would leave possibly many once active galaxies without a retinue of associated quasars within $30'$.

From the batteries of curves shown in Figure 12 we make the following observations about the comparison of the quasar family detection results for bright versus faint SDSS quasars with SDSS galaxies and with 2MRS galaxies.

9. The sigma values shown in Figure 12 are reduced relative to those shown in Figure 3. This is expected since each test used only about two fifths of the input quasar data set, but it is also the case that quasar families detected in the original tests have a decreased likelihood of survival in the bright/faint tests if they include quasars from more than one magnitude range. It is in any case clear from Figure 12 that the curve envelope averages in each selected magnitude range maintain very high significance ($\sigma \gtrsim 20$ for $0.002 \leq |z_v|_{max} \leq 0.030$ for SDSS galaxies; $\sigma \gtrsim 10$ for $0.010 \leq |z_v|_{max} \leq 0.030$ for 2MRS galaxies). The curve envelopes exhibited for SDSS and 2MRS tests in Figure 3 are maintained in Figure 12 for both bright and faint SDSS quasars, and, although the 2MRS envelope is somewhat more ragged for the bright/faint tests, the bright and faint curves cross at various points over the $|z_v|_{max}$ range, so the results for bright and faint quasars are comparable both for SDSS galaxies and for 2MRS galaxies.

7.1. Quasars around 2MRS Galaxies versus around SDSS Galaxies

In Paper I we noted that the overlap that exists between fields of quasars that are within reach of two or more galaxies makes it difficult to analyze redshift fields based on an ejection hypothesis. This difficulty should be less pronounced for putative parent galaxies that are nearby, and this is consistent with the above observations. However, there are additional observations that can be made about the detection of quasars associated with nearby versus distant galaxies.

The quasars detected as members of families around 2MRS galaxies are for the most part not also detected as members of families around *different* SDSS galaxies and vice versa, a clear indication that the detection algorithm distinguishes between nearby and more distant galaxies and their respective quasar families. Table 8 presents a quantitative comparison of the quasars detected around 2MRS versus around SDSS galaxies for the respective tests done with $\Delta z_g = 0.015$ and $|z_v|_{\max} = 0.030$. More than half (53.7%) of the quasars detected around 2MRS galaxies are not detected around SDSS galaxies. For the remaining quasars (46.3%) detected in both tests, if the parent galaxies have proximity within $30''$ and redshifts within $\delta z = 0.010$, the galaxies are deemed identical (6.6%). Since the 2MRS and SDSS galaxy input data sets were declustered separately, the same declustering must now be applied, so the non-identical parent galaxy pairs are deemed declustered (15.6%) if they have proximity within $30'$ and redshifts within $\delta z = 0.010$. The remaining galaxy pairs are deemed different (24.0%), leaving three quarters of the quasar detections as being in association only with a 2MRS galaxy.

Table 8: SDSS Quasars Detected around 2MRS vs. around SDSS Galaxies for Tests Done with $\Delta z_g = 0.015$ and $|z_v|_{\max} = 0.030$

Detections	Count	% around 2MRS Galaxies
Quasars around 2MRS galaxies (in sample)	454	100.0
Quasars around SDSS galaxies (in sample)	4,525	...
Quasars around 2MRS galaxies only	244	53.7
Quasars around 2MRS and SDSS galaxies	210	46.3
Galaxies identical	30	6.6
Galaxies declustered	71	15.6
Galaxies different	**109**	**24.0**

The quasar detections around 2MRS galaxies also exhibit another important difference.

The tests for the 2MRS and SDSS curves shown in Figure 3 for $\Delta z_g = 0.015$ were repeated *without* quasar uniqueness enforced in order to record the respective percentages of unique quasar family member detections. As shown in Figure 13, the uniqueness percentages for 2MRS galaxies (black) exceed 93% on average, whereas the percentages for SDSS galaxies (gray) are comparable only for very tight values of $|z_v|_{\max}$ and drop off precipitously as $|z_v|_{\max}$ increases, i.e. detection of uniquely associated quasars is largely inherent around nearby galaxies and increasingly difficult around more and more distant galaxies. The high inherent SDSS quasar uniqueness for 2MRS galaxies is in fact the reason that, as discussed in Items 3 and 5 in §7, the periodicity signal drops off asymptotically to a constant but robust value, as opposed to dropping off to no signal when the input data set, 2dF or SDSS, includes more distant galaxies.

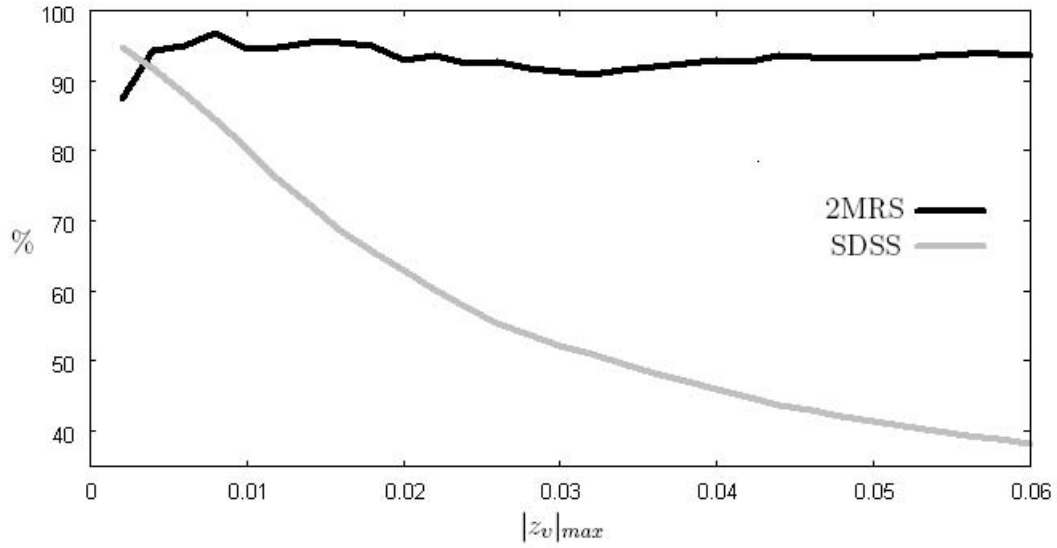

Fig. 13.— Comparison of percentage of inherent SDSS quasar uniqueness around 2MRS galaxies vs. around SDSS galaxies.

7.2. Quasar Excess at Karlsson Redshifts

If Karlsson periodicity in conjunction with the ejection hypothesis is correct, there may be an expectation that there exists a detectable excess of quasars with redshifts at or near Karlsson redshifts. There is evidence by position, as opposed to redshift, of very low levels of quasar excess and paucity around galaxies, which is attributed by Scranton et al. (2005) to gravitational lensing, but since the periodicity signal we detect is so strong, one might expect that this signal is already an indication that an excess at Karlsson redshifts exists. To detect a quasar excess, we tracked the frequency of close proximity of quasar z_0 values to Karlsson peaks. Proximity, being the first determiner of whether or not a given quasar is in excess, is the deviation of the quasar z_0 from the closest Karlsson redshift z_K, so the computation of the proximity is the same as that for z_v, as defined at the end of §5. This is convenient because z_v is always computed by the detection algorithm and it is already the subject of the $|z_v|_{\max}$ constraint. The next consideration for each of the quasars in proximity is whether or not the quasar is also a member of a detected family. Using our detection method, a *non*-member quasar is *not* counted as being in excess. The measure of the quasar excess at Karlsson redshifts, then, for an entire data set, is the number of quasars that are accepted by the $|z_v|_{\max}$ constraint *and* that succeed in becoming a member of a detected family.

With the above accounting procedure in place, a normal test will determine the total number of quasars in excess at Karlsson redshifts, and this will be a measurement corresponding to the applied constraints for the test, with the proximity being explicitly specified by the $|z_v|_{\max}$ constraint. This gives us an overall count of excess quasars for a given proximity, but in order to assign meaning to this count, we need a number to which it can be compared and we need to determine the statistical significance of the result. Both needs can be met by invoking a control, just as we have done for quasar family detection. The normal and control numbers can then be plugged into the equation used for the computation of σ. In the presence of a positive signal for quasar families, the control will generate fewer family hits than the normal, but this disparity is easily taken into account by normalizing the control hits to the normal hits, resulting in a revised computation for the excess sigma: $\sigma_e = (((\mathsf{e}_{\text{normal}} - \mathsf{e}_{\text{control}})/\sqrt{\mathsf{e}_{\text{control}}}) * (\mathsf{hits}_{\text{control}}/\mathsf{hits}_{\text{normal}}))$, where e is the excess and σ_e is the significance of the excess. With this quasar excess logic in place, we ran test batteries to determine the quasar excess at Karlsson redshifts for the SDSS, 2MRS, and 2dF data sets. All tests were run with $\Delta z_g = 0.015$, $|z_v|_{\max} = 0.002$ through 0.120 in increments of 0.002, and *all* of the Karlsson corollary constraints. Figure 14 shows that there is a very strong quasar excess at Karlsson redshifts for all three data sets. The excess signal for SDSS is much higher than for 2MRS or 2dF because, as with the quasar family detection signal, the quasar excess signal increases with object population size.

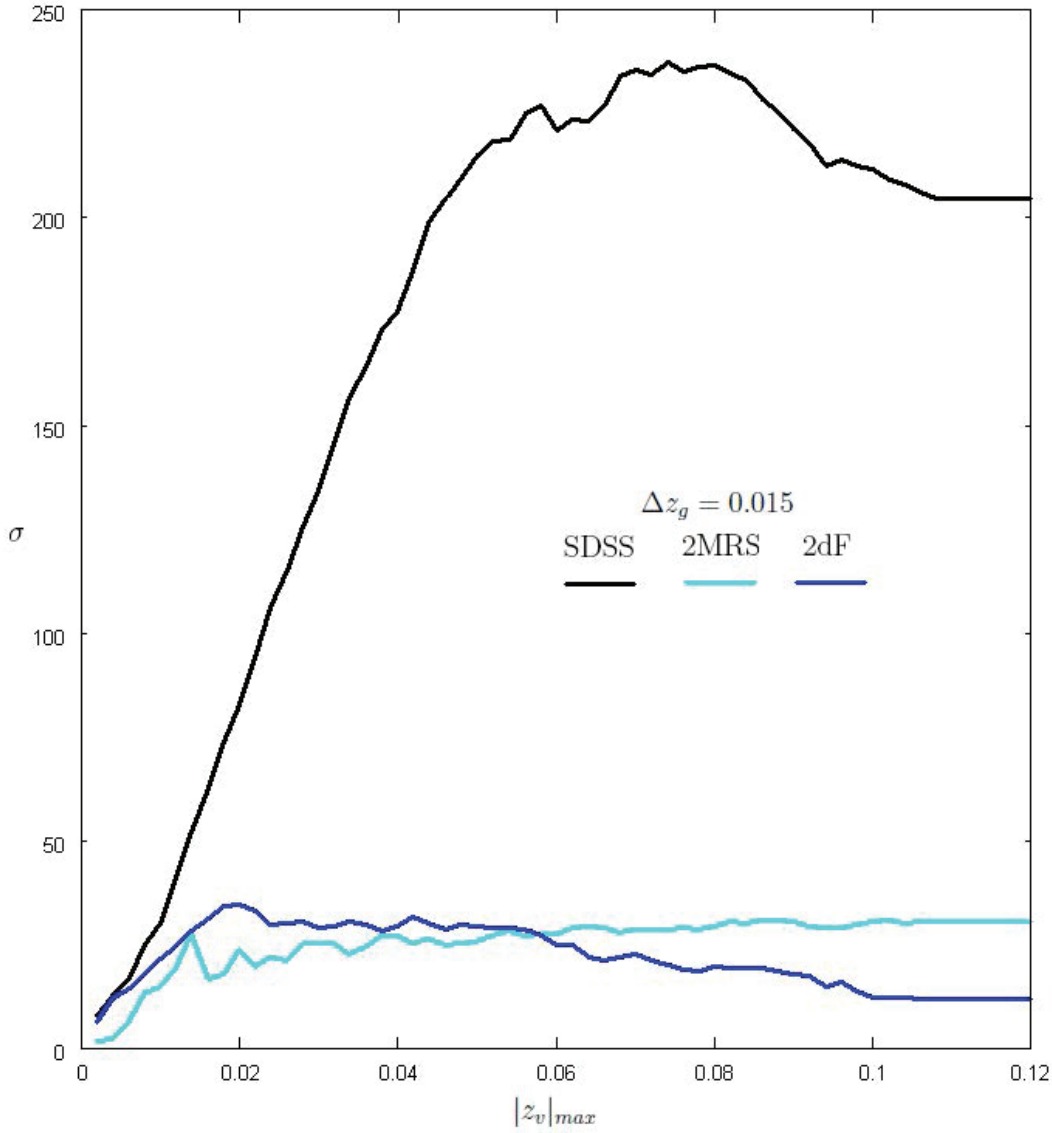

Fig. 14.— Quasar excess at Karlsson redshifts. All curves are for tests run with $\Delta z_g = 0.015$, $|z_v|_{\max} = 0.002$ through 0.120 in increments of 0.002, and the Karlsson corollary constraints.

7.3. Using Galaxy Random Redshifts For The Control

In Paper I §4.2 we invoked a control that randomized the redshifts of the galaxies, rather than the quasars, using redshifts from the pool of all 2dFGRS galaxy redshifts. The purpose, as proposed by the Paper I referee, was to make the quasars lose track of the galaxies from which they were ejected, thus demonstrating that our result was not due to a selection effect. However, we faced a conundrum, because there are numerous methods of implementing the proposal. One method is to perform our test as usual, i.e. have the normal use actual quasar redshifts and the control use randomized quasar redshifts, but in each case also randomize the galaxy redshifts. One can argue that this comparison is flawed because there are multiple sets of redshifts being randomized, one in the normal and both in the control, thus possibly destroying any actual relationship between the data sets, within the control, and between the normal and control. Other variations on this method are available, but each has a downside with regard to multiple randomized data sets in the same test.

A very clean method is to maintain the status quo for the normal versus control relationship by keeping the normal as is and having the control use randomized redshifts for the putative parent galaxies, rather than using randomized redshifts for the quasars. For Paper I, we selected this method, and this seemed to yield the expected result, i.e. no signal, but with a caveat. The test batteries revealed a possible signal at the 3 or 4σ level, but because this signal was marginal and because it was far outweighed by the test batteries that used the quasar random redshift control, we argued for the lack of a selection effect. Now, since the SDSS data set is at least an order of magnitude larger than the 2dF data set, we can explore the signal further to determine whether a selection effect may exist and, separately, to establish whether the galaxies, not just the quasars, can generate a signal. As in Paper I, we used a test battery that invokes the galaxy redshift randomization just described, using raw galaxy redshifts. For comparison we used $\Delta z_g = 0.015$ for the redshift grouping constraint and $|z_v|_{\max} = 0.002$ through 0.120 in increments of 0.002 for the redshift velocity constraint. The curves in Figure 15 show the results. The black curves are for tests done with no Karlsson corollary constraints (the lightest black curve) and with one or more Karlsson corollary constraints (the increasingly heavy black curves). Although the signal is unmistakeable, its maximum of $\sigma \simeq 52$ is less than a third of the signal maximum of $\sigma \simeq 166$ produced by the same tests done with the randomized quasar redshift control. Manifestation of the signal requires a very large galaxy/quasar data set, with the signal rising in direct proportion to both object populations, in this case by an order of magnitude from 3 or 4σ for 2dF to 40 or 50σ for SDSS. We must conclude that there is indeed a signal when using the galaxy random redshift control, albeit not as clear cut as with the quasar random redshift control. We maintain that the same test also argues for the lack of a selection effect, but on the basis that *both* galaxies and quasars, independently, can produce the signal.

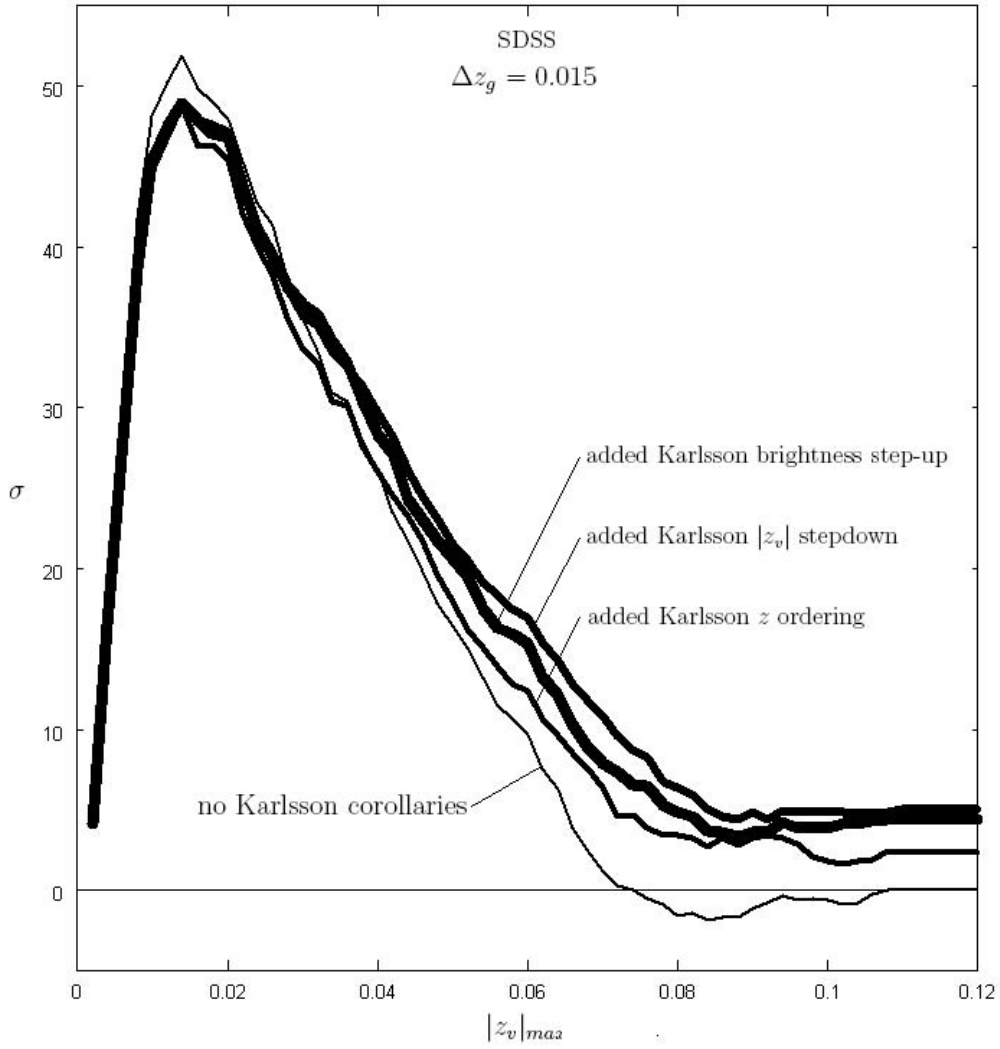

Fig. 15.— Effect of constraints on σ for the SDSS data set when using galaxy random redshifts instead of quasar random redshifts, as explained in §7.3. The increasingly heavy black curves are for tests run first with $\Delta z_g = 0.015$ and no Karlsson corollary constraints, second with addition of the Karlsson z ordering constraint, third with addition of the Karlsson $|z_v|$ stepdown constraint, and finally with addition of the Karlsson brightness step-up constraint.

8. EFFECT OF TEST CONSTRAINTS ON THE PERIODICITY SIGNAL

Here we show the results of tests with constraints in various configurations to show the relative effects of the constraints on the periodicity signal. We proceeded with $N_{\rm min} = 2$ as usual and used $\Delta z_g = 0.015$ for the redshift grouping constraint when that constraint is applied. Figures 16 and 17, respectively, show the results for the SDSS and 2MRS data sets. The black curves are for tests done with no Karlsson corollary constraints (the lightest solid black curve) and with one or more Karlsson corollary constraints (the increasingly heavy black curves). The lightest solid black curve in each figure represents a mid-envelope assessment of the strong signal exhibited by quasar families, and this signal is derived solely by constraining only two parameters, one constraint insisting on at least two quasar candidates with similar redshifts, here within $\Delta z_g = 0.015$, and the other constraint insisting on a maximum ejection velocity in z_v-space, $|z_v|_{\rm max}$. Within this regime for SDSS, the strongest signal occurs at $|z_v|_{\rm max} \simeq 0.006$ ($1,800$ km s^{-1}) and the signal remains robust out to $|z_v|_{\rm max} \simeq 0.030$ ($9,000$ km s^{-1}). For 2MRS, the respective numbers are almost the same, with the strongest signal at $|z_v|_{\rm max} \simeq 0.022$ ($6,600$ km s^{-1}). If we consider only this regime, i.e. $|z_v|_{\rm max} \leq 0.030$, it appears that on statistical average, quasars are ejected with a maximum velocity of $\simeq 9,000$ km s^{-1}. However, it must be kept in mind that this result does not dictate a maximum velocity for all ejected quasars. For the 2MRS (nearby) galaxies, for which quasar family detection is facilitated by galaxy nearness (see §7.1), the ejection velocity is inconsequential when it exceeds $\simeq 0.110$ ($33,000$ km s^{-1}). Note that all of the curves in Figure 17 are flat to infinity beyond this value, and that when the Karlsson corollary constraints are also applied, the signal, for all values of $|z_v|_{\rm max}$, is markedly strengthened with each additional corollary constraint applied.

We also demonstrate the efficacy of the Δz_g constraint, the Karlsson corollary constraints, and the quasar redshift transformation. The heavy solid gray curve in each figure is for tests run with $\Delta z_g = 0.015$ and all of the Karlsson corollaries, but with the sense of the Δz_g constraint inverted, i.e. the quasars are *rejected* as companions if they are grouped in redshift. As expected, if the redshift grouping constraint is efficacious when applied normally, the inverted constraint produces an anti-correlation for both SDSS and 2MRS in the range of the strongest respective signal, with negative maxima at $\sigma \simeq -16$ for SDSS and $\sigma \simeq -7$ for 2MRS. For maximum ejection velocities above $|z_v|_{\rm max} \simeq 0.040$ ($12,000$ km s^{-1}), the inversion merely suppresses the signal for both SDSS and 2MRS, and for the 2MRS this includes suppression of any effect of the Karlsson corollaries, which is consistent with the corollaries being routinely handed quasars that are not viable association candidates. For SDSS we show two additional anti-correlations, one with the Karlsson corollaries (gray dash-dot curve) and one without (gray dashed curve), but both *without* transforming the quasar redshifts, actual or random, to the rest frame of the putative parent galaxy.

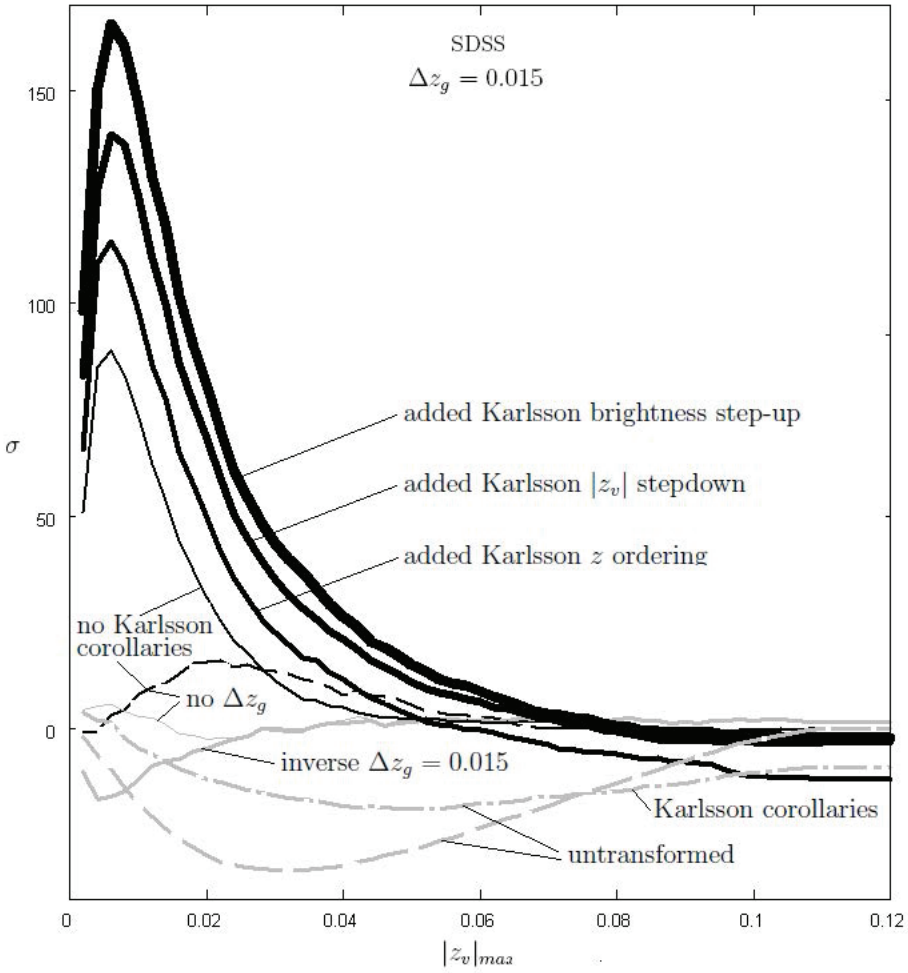

Fig. 16.— Effect of constraints on σ for the SDSS data set when using or not using the Δz_g constraint and the Karlsson corollary constraints. The increasingly heavy black curves are for tests run first with $\Delta z_g = 0.015$ and no Karlsson corollary constraints, second with addition of the Karlsson z ordering constraint, third with addition of the Karlsson $|z_v|$ stepdown constraint, and finally with addition of the Karlsson brightness step-up constraint, the latter configuration making up the complete constraint set used throughout the paper. The dashed black curve is for tests run with no Δz_g constraint and no Karlsson corollaries. The lighter gray curve is for tests run with all of the Karlsson corollaries but no Δz_g constraint. The heavy solid gray curve is for tests run with $\Delta z_g = 0.015$ and all of the Karlsson corollaries, but with the sense of the Δz_g constraint inverted, i.e. the quasars are *rejected* as companions if they are grouped in redshift. The gray dash-dot and dashed curves are for tests run respectively with or without the Karlsson corollaries but *without* transforming the quasar redshifts, actual or random, to the rest frame of the putative parent galaxy.

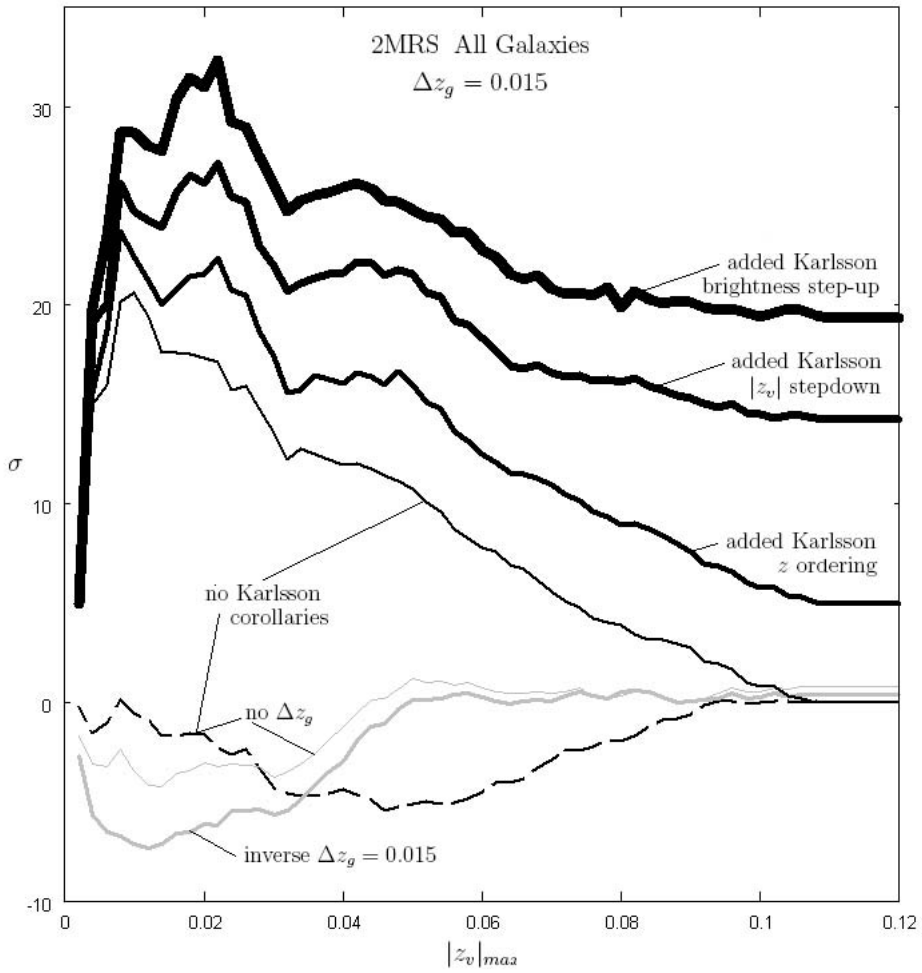

Fig. 17.— Effect of constraints on σ for the 2MRS data set when using or not using the Δz_g constraint and the Karlsson corollary constraints. The increasingly heavy black curves are for tests run first with $\Delta z_g = 0.015$ and no Karlsson corollary constraints, second with addition of the Karlsson z ordering constraint, third with addition of the Karlsson $|z_v|$ stepdown constraint, and finally with addition of the Karlsson brightness step-up constraint, the latter configuration making up the complete constraint set used throughout the paper. The dashed black curve is for tests run with no Δz_g constraint and no Karlsson corollaries. The lighter gray curve is for tests run with all of the Karlsson corollaries but no Δz_g constraint. The heavy solid gray curve is for tests run with $\Delta z_g = 0.015$ and all of the Karlsson corollaries, but with the sense of the Δz_g constraint inverted, i.e. the quasars are *rejected* as companions if they are grouped in redshift.

8.1. Two Quasar Minimum and Redshift Grouping

We should note that the two quasar minimum per quasar family does *not* contribute to the signal that we detect, *nor* does the redshift grouping constraint. Each is only a fulcrum. When they are used together and in combination with other constraints they allow the signal to become manifest. If we run a test with $N_{\min} = 2$ and apply no constraints, the control will pass through the same quasars that the normal does, yielding a normal to control parent galaxy hit ratio identically equal to 1, i.e. a completely noiseless null signal. If we run the same test but also apply any value of the Δz_g constraint, the normal and control will allow only certain quasars to pass through the constraint, but these quasars will be the *same* for the normal and control for each putative parent galaxy, as already described in Table 2 and §5, again yielding a normal to control parent galaxy hit ratio identically equal to 1. Consequently, the entire range of significance of our result, not just the extremely high portion, comes purely from the $|z_v|_{\max}$ constraint plus any Karlsson corollary constraints that are applied.

The redshift grouping constraint works against actual rather than random redshifts for the control, but although the normal and control will therefore each pass exactly the same quasars through the Δz_g constraint, the control will use random redshifts for these quasars when processing any other constraints. One might therefore be concerned that the control is at a disadvantage when, for example, the $|z_v|_{\max}$ constraint is applied to quasar random redshifts for which the Karlsson redshift, z_k, selected by the algorithm is not the same for the control as for the normal. However, this is demonstrably not the case. We ran a test battery using $\Delta z_g = 0.015$, $|z_v|_{\max} = 0.002$ through 0.120 in increments of 0.002, and no Karlsson corollary constraints. For the normal and control, independently of the usual accounting, we recorded the number of acceptances and rejections produced by the $|z_v|_{\max}$ constraint, and for the control, we subdivided the acceptances and rejections into those that used the *same* Karlsson peak as the normal, as opposed to those that used a *different* Karlsson peak. Figure 18 shows the SDSS signal and the percentage of accepted quasars out of all candidate quasars tested by the $|z_v|_{\max}$ constraint, with separate curves for the normal acceptance percentage, the control acceptance percentage for the case where the algorithm selects the *same* z_k as the normal, and the control acceptance percentage for the case where the algorithm selects a z_k for the control that is *different* from that selected for the normal. For every value of $|z_v|_{\max}$, the sum of the two control percentages is very nearly equal to (within 0.20 percent of) the normal percentage, i.e. the control is not at a disadvantage if the Karlsson peak selected is not the same as that selected for the normal. The control is quite capable of having, and more often than not does have, quasars accepted by the $|z_v|_{\max}$ constraint with random redshifts that are disparate from the actual redshifts used by the normal. The Δz_g constraint is completely decoupled from the $|z_v|_{\max}$ or any other constraint. The 2MRS test

battery produces the same percentages.

Figure 18 provides a definitive explanation of the behavior of the signal with $N_{\rm min} = 1$ versus $N_{\rm min} = 2$. That the control is nearly equal to the normal in having individual quasars accepted by the $|z_v|_{\rm max}$ constraint is expected due to two ambiguities (Paper I §4.1) that arise when applying the ejection hypothesis, one being that many of the quasars are within reach of more than one galaxy, i.e. family overlap, and the other being that any given redshift has a very good chance of meeting a criterion based on the computed value of z_v, i.e. within $z_v \sim \pm 0.1$. In addition, the actual or random redshifts of any accepted quasars need not be close to one another, and none of the constraints depend in any way on the value of $N_{\rm min}$. Consequently, if the signal does exist and $N_{\rm min}$ is equal to 1 for a given constraint set, the signal will not be manifest, which is the result we obtain for this case. On the other hand, if the signal does exist and $N_{\rm min}$ is *greater* than 1 for the same constraint set, the normal and control will still each respectively have exactly the same quasars accepted as they do for the $N_{\rm min} = 1$ case, but each is now under an edict to supply more than one such quasar to achieve a family detection. By hypothesis then, the normal has the advantage because it is using actual rather than random redshifts, so the signal will be manifest, which again is the result we obtain. These results quantitatively assert the existence of both the family overlap and the strong signal with $N_{\rm min} = 2$.

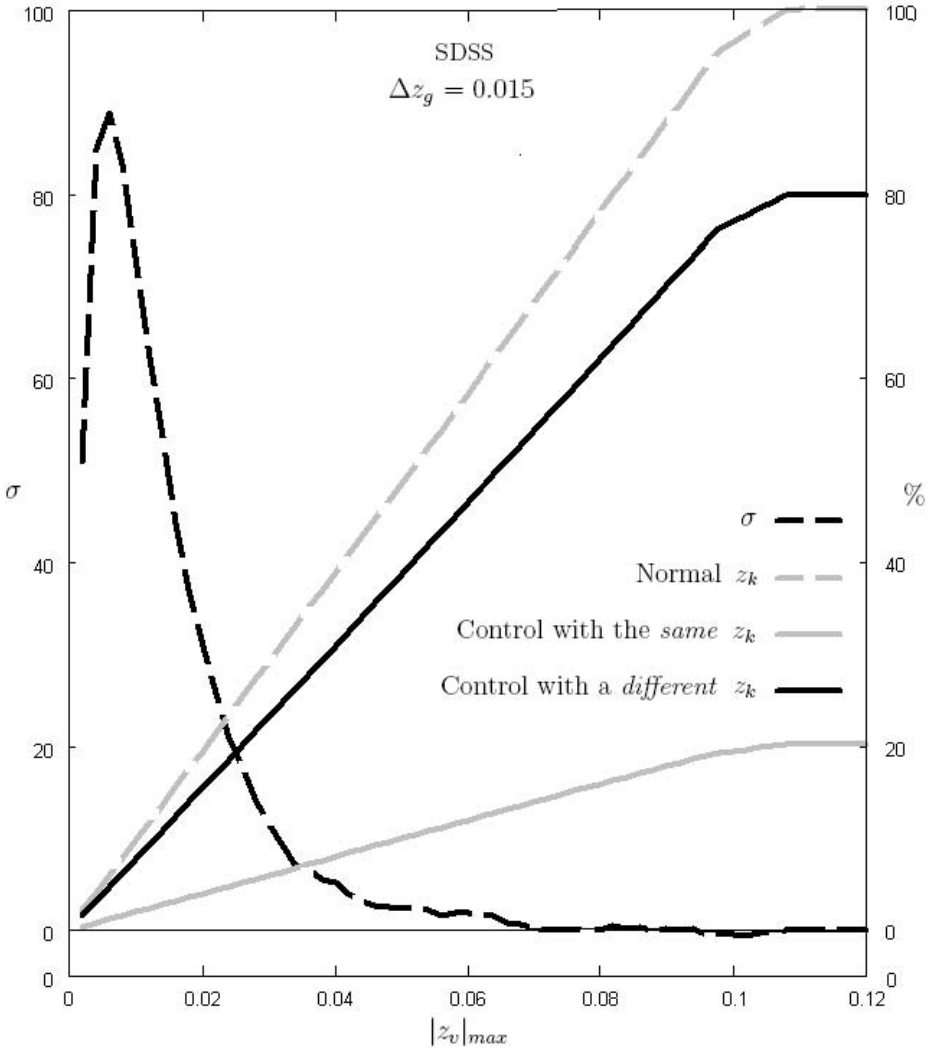

Fig. 18.— The SDSS z maximum velocity signal and its normal and control acceptance percentages, as explained in §8.1. All curves are for tests run with $\Delta z_g = 0.015$, $|z_v|_{\max} = 0.002$ through 0.120 in increments of 0.002, and no Karlsson corollary constraints. The dashed black curve shows the signal. The remaining curves show the percentage of accepted quasars out of all candidate quasars tested by the $|z_v|_{\max}$ constraint for the Karlsson redshift, z_k, selected by the algorithm. The normal acceptance percentage curve is dashed gray. The control acceptance percentage curve is solid gray for the case where the algorithm selects the *same* z_k as the normal for the control. The control acceptance percentage curve is solid black for the case where the algorithm selects a z_k for the control that is *different* from that selected for the normal. The sum of the two control percentages is at every point equal to the normal percentage.

8.2. Redshift Grouping versus the Non-grouping Constraints

In §8.1 we tallied quasar acceptance and rejection counts for the $|z_v|_{\max}$ constraint and used this information to generate Figure 18. We used a similar technique to unravel the actual detailed behaviors and effects of each of the key constraints when used alone or in concert. In this case we tallied the quasar rejections as before, but we also separately tallied the number of applications of each constraint so that we could measure quasar rejections by a constraint as a percentage of total applications of that constraint, and we implemented this tally for the $|z_v|_{\max}$ constraint, the Δz_g constraint, the quasar uniqueness criterion, and all combinations of these three applications.

An essential point to note about this experiment is that counts of individual rejected quasars as companions do not, by themselves, measure whether a given possible quasar family produces a hit. In terms of constraints, the fate of any given candidate quasar within $30'$ of a galaxy is completely independent of the fate of any of the other candidate quasars so positioned. The uniqueness criterion can disqualify a quasar, but this occurrence is not constraint-based because it happens only when a given quasar has already been detected as a family member for more than one galaxy. If a given quasar is rejected for any reason, but the putative parent galaxy scores a hit, the rejection of that particular quasar is inconsequential in terms of the ability of the control to garner quasar family hits relative to the normal. Therefore, in order to weigh the true effect of quasar rejections, the rejection versus application tallies must be incremented *only* when the putative parent galaxy does *not* produce a hit. We implemented this rule in the tally algorithm.

We tallied the rejections and the number of applications of each constraint. Then, for each constraint and for each combination of constraints, we computed the rejections as a percentage of the total applications of each constraint in order to obtain the percent differences between the normal and the control. The percent differences are plotted along with the sigma in Figure 19. This provides an in depth look at how the constraints are playing out for the normal relative to the control in terms of quasars being rejected as companions. When the percent difference ($\Delta\%$) is positive, as with the warm colored curves, the normal quasars are being rejected slightly more often than the control quasars, and when negative, as with the cool colored curves, the control quasars are being rejected slightly more often. The meanings of the colored curves are as follows:

- The green curve represents rejections by the $|z_v|_{\max}$ constraint only. This curve is decidedly below $\Delta\% = 0$ and shows that this constraint when acting alone does indeed produce a signal that is masked when quasar rejections are considered without regard to whether or not a quasar family hit is produced by some other candidate quasars

that are not rejected.

- The gray curve represents rejections by the Δz_g constraint only. This curve rests at $\Delta\% \equiv 0$ at every point because the normal and control rejection counts are *always* identical to each other.

- The brown curve represents rejections by the *not unique* criterion only, which rejects any quasar that is detected as a family member of more than one galaxy. This is a criterion rather than a constraint because it is enforced only after a quasar has been detected as a member of a quasar family that might otherwise have scored a hit based on the first pass of the detection algorithm. Consequently, the counts represented by the brown curve, though legitimate as measurements, are not equivalent to the counts represented by the curves for the other constraints or constraint combinations.

- The cyan curve represents rejections by both the $|z_v|_{\max}$ constraint and the Δz_g constraint. Like the green curve, this curve is decidedly below $\Delta\% = 0$ and shows that when these constraints operate in tandem they unmask the signal that is actually produced by the $|z_v|_{\max}$ constraint.

- The red curve represents rejections by both the $|z_v|_{\max}$ constraint and the not unique criterion.

- The purple curve represents rejections by both the Δz_g constraint and the not unique criterion.

- The magenta curve represents rejections by the $|z_v|_{\max}$ constraint, the Δz_g constraint, and the not unique criterion.

The percentage differences of the cool curves are small, averaging ~ 1 percent at mid-range significance, but they are detectable because the input data sets are extremely large. The green curve unequivocally declares the existence of the signal and by extension the very high sigmas achieved declare the robustness of the signal. The cyan curve ramps up emphatically relative to the green curve, demonstrating the boost in and consequent unmasking of the signal that results from filtering out interloping quasars. In each case, the control is at a disadvantage only because it is not working with actual redshifts.

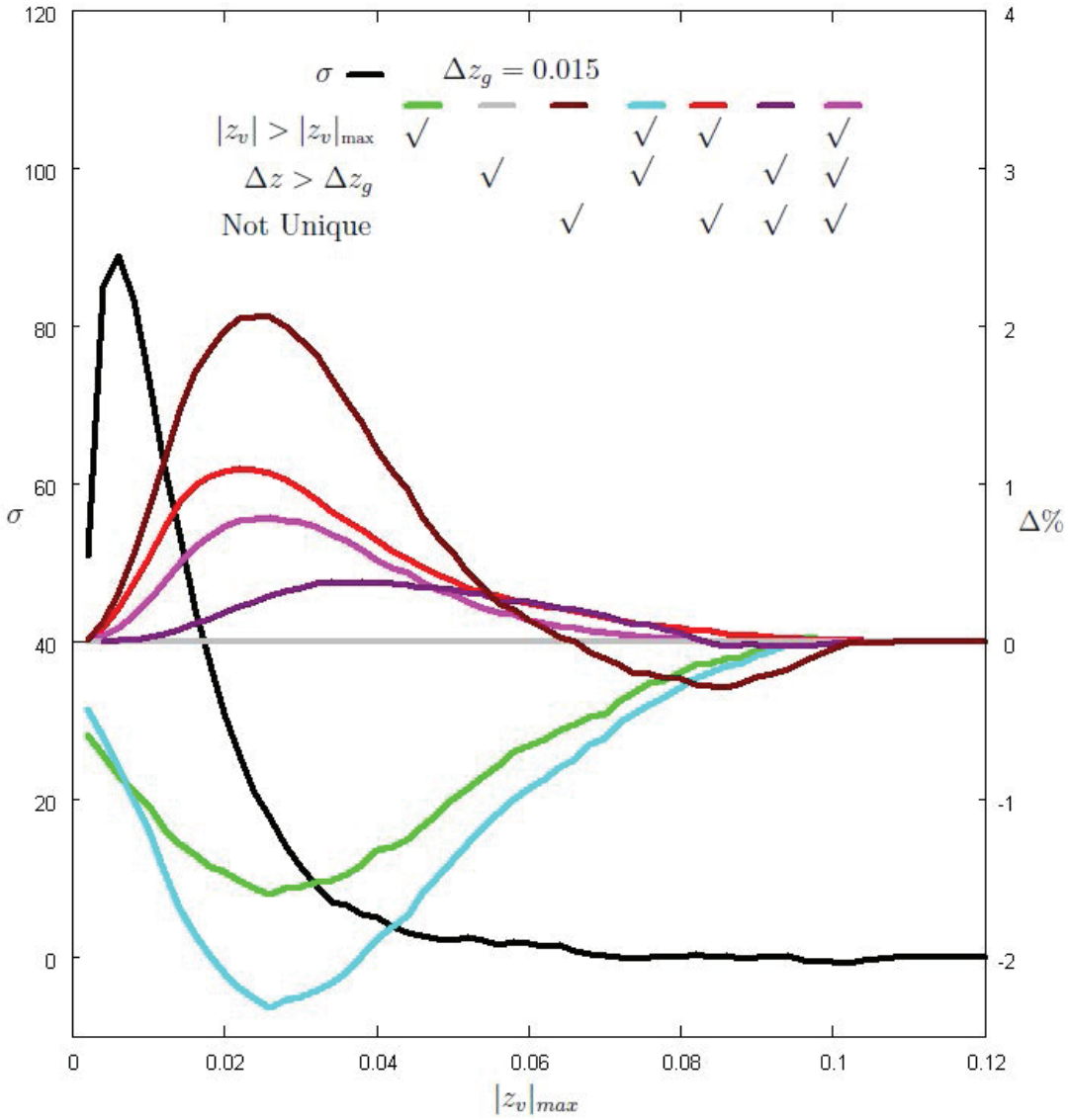

Fig. 19.— The SDSS signal (black curve) and constraint rejection versus application percent differences (colored curves) for different combinations of the constraint set with and without the quasar uniqueness criterion, the $\Delta z_g = 0.015$ constraint, and the $|z_v|_{\rm max}$ constraint, in all combinations, and with *no* Karlsson corollary constraints. The warm colored curves demonstrate the tendency of the control to prevail over the normal in scoring quasar family hits, and the cool colored curves demonstrate the tendency of the normal to prevail over the control.

9. CONCLUSIONS

In Paper I we concluded that, at least for the 2dF data set, certain quasars are physically associated with lower redshift galaxies by virtue of quasar redshifts with an implied ejection velocity component and a large intrinsic non-velocity component. The results presented in this paper lead us to conclude that: similarly, certain SDSS quasars are physically associated with lower redshift SDSS galaxies and separately with lower redshift 2MRS galaxies; at least some quasars of very different redshift are physically associated with the same nearby galaxy; with the available typed galaxy data, quasar families occur with approximately equal frequency around nearby ellipticals and lenticulars versus around nearby spirals and irregulars, and quasar families occur somewhat more frequently around nearby unbarred spirals than around nearby barred spirals.

When analyzed separately, the bright and faint quasars maintain high and comparable detection significance around both nearby and distant galaxies, suggesting that gravitational lensing is an unlikely physical explanation for the signal that we detect.

A quasar excess exists at Karlsson redshifts around the 2dF, SDSS, and 2MRS galaxies.

For this paper, we made use of a number of resources. Funding for the SDSS and SDSS-II has been provided by the Alfred P. Sloan Foundation, the Participating Institutions, the National Science Foundation, the U.S. Department of Energy, the National Aeronautics and Space Administration, the Japanese Monbukagakusho, the Max Planck Society, and the Higher Education Funding Council for England. The SDSS Web Site is http://www.sdss.org/.

The SDSS is managed by the Astrophysical Research Consortium for the Participating Institutions. The Participating Institutions are the American Museum of Natural History, Astrophysical Institute Potsdam, University of Basel, University of Cambridge, Case Western Reserve University, University of Chicago, Drexel University, Fermilab, the Institute for Advanced Study, the Japan Participation Group, Johns Hopkins University, the Joint Institute for Nuclear Astrophysics, the Kavli Institute for Particle Astrophysics and Cosmology, the Korean Scientist Group, the Chinese Academy of Sciences (LAMOST), Los Alamos National Laboratory, the Max-Planck-Institute for Astronomy (MPIA), the Max-Planck-Institute for Astrophysics (MPA), New Mexico State University, Ohio State University, University of Pittsburgh, University of Portsmouth, Princeton University, the United States Naval Observatory, and the University of Washington.

The 2MRS builds and improves on the large redshift surveys of the nearby universe as outlined in Table 1 of Huchra et al. (2012).

The 2dFGRS survey was compiled by the 2dFGRS survey team from observations made with the Two-Degree Field on the Anglo-Australian Telescope (AAT). We used the 2dFGRS survey mask files and a *C* translation of the 2dFGRS mask software written in FORTRAN by Peder Norberg and Shaun Cole (University of Durham, UK) of the 2dFGRS team.

The 2QZ survey was compiled by the 2QZ survey team from observations made with the Two-Degree Field on the AAT. We used the 2QZ survey mask files and formats produced by Robert Smith (Liverpool John Moores University, UK) and Scott Croom (AAO; University of Sydney, Australia).

This is a post-peer-review, pre-copyedit version of an article published in Astrophysics and Space Science. The final authenticated version is available online at: http://dx.doi.org/10.1007/s10509-018-3355-5.

REFERENCES

Abazajian, K. N., Adelman-McCarthy, J. K., Agüeros, M. A., et al. 2009, ApJS, 182, 543

Croom, S. M., Smith, R. J., Boyle, B. J., et al. 2001, MNRAS, 322, 29

Fulton, C. C., & Arp, H. C. 2012, ApJ, 754, 134 (Paper I)

Hartnett, J. G. 2009, Ap&SS, 324, 13

Huchra, J. P., Macri, L. M., Masters, K. L., et al. 2012, ApJS, 199, 26

Karlsson, K. G. 1971, A&A, 13, 333

Karlsson, K. G. 1973, Nature Phys. Sci., 245, 68

Karlsson, K. G. 1977, A&A, 58, 273

Narlikar, J., & Arp, H. 1993, ApJ, 405, 51

Richards, G. T., Xiaohui, F., Newberg, H. J., et al. 2002, AJ, 123, 2945

Sadler, E. M., Jackson, C. A., Cannon, R. D., et al. 2002, MNRAS, 329, 227

Schneider, D. P., Richards, G. T., Hall, P. B., et al. 2010, AJ, 139, 2360

Scranton, R., Ménard, B., Richards, G. T., et al. 2005, ApJ, 633, 589

Shen, Y., Richards, G. T., Strauss, M. A., et al. 2011, ApJS, 194, 45

Skrutskie, M. F., Cutri, R. M., Stiening, R., et al. 2006, AJ, 131, 1163

York, D. G., Adelman, J., Anderson, J. E., Jr., et al. 2000, AJ, 120, 1579

This preprint was prepared with the AAS LaTeX macros v5.2.